ISSN 1674-1056
http://cpb.iphy.ac.cn
http://iopscience.iop.org/cpb
中国物理 B
Chinese Physics
中国物理 Chinese Physics B

Promise of commercialization:carbon materials for low-cost perovskite solar cells

Yu Cai(蔡宇), Lusheng Liang(梁禄生), Peng Gao(高鹏)
Citation: Chin. Phys. B . 2018, 27(1): 018805. **doi:** 10.1088/1674-1056/27/1/018805

Journal homepage: http://cpb.iphy.ac.cn; http://iopscience.iop.org/cpb

What follows is a list of articles you may be interested in

TiO_2 composite electron transport layers for planar perovskite solar cells by mixed spray pyrolysis with precursor solution incorporating TiO_2 nanoparticles

Jiaqi Tian(田嘉琪), Hongcui Li(李红翠), Haiyue Wang(王海月), Bo Zheng(郑博), Yebin Xue(薛叶斌), Xizhe Liu(刘喜哲)
Chin. Phys. B . 2018, 27(1): 018810. **doi:** 10.1088/1674-1056/27/1/018810

420 nm thick $CH_3NH_3PbI_{3-x}Br_x$ capping layers for efficient TiO_2 nanorod array perovskite solar cells

Long Li(李龙), Cheng-Wu Shi(史成武), Xin-Lian Deng(邓新莲), Yan-Qing Wang(王艳青), Guan-Nan Xiao(肖冠南), Ling-Ling Ni(倪玲玲)
Chin. Phys. B . 2018, 27(1): 018804. **doi:** 10.1088/1674-1056/27/1/018804

O_3 fast and simple treatment-enhanced p-doped in Spiro-MeOTAD for CH_3NH_3I vapor-assisted processed $CH_3NH_3PbI_3$ perovskite solar cells

En-Dong Jia(贾恩东), Xi Lou(娄茜), Chun-Lan Zhou(周春兰), Wei-Chang Hao(郝维昌), Wen-Jing Wang(王文静)
Chin. Phys. B . 2017, 26(6): 068803. **doi:** 10.1088/1674-1056/26/6/068803

Simulation design of P-I-N-type all-perovskite solar cells with high efficiency

Hui-Jing Du(杜会静), Wei-Chao Wang(王韦超), Yi-Fan Gu(顾一帆)
Chin. Phys. B . 2017, 26(2): 028803. **doi:** 10.1088/1674-1056/26/2/028803

Device simulation of lead-free $CH_3NH_3SnI_3$ perovskite solar cells with high efficiency

Hui-Jing Du(杜会静), Wei-Chao Wang(王韦超), Jian-Zhuo Zhu(朱键卓)
Chin. Phys. B . 2016, 25(10): 108802. **doi:** 10.1088/1674-1056/25/10/108802

TOPICAL REVIEW — New generation solar cells

Promise of commercialization: Carbon materials for low-cost perovskite solar cells*

Yu Cai(蔡宇)[1,2], Lusheng Liang(梁禄生)[2], and Peng Gao(高鹏)[2,†]

[1] Department of Chemistry, Fujian Normal University, Fuzhou 350007, China
[2] Laboratory for Advanced Functional Materials, Xiamen Institute of Rare-earth Materials, Chinese Academy of Science, Xiamen 361021, China

(Received 2 October 2017; revised manuscript received 21 November 2017; published online 13 December 2017)

Perovskite solar cells (PVSCs) have attracted extensive studies due to their high power conversion efficiency (PCE) with low-cost in both raw material and processes. However, there remain obstacles that hinder the way to their commercialization. Among many drawbacks in PVSCs, we note the problems brought by the use of noble metal counter electrodes (CEs) such as gold and silver. The costly Au and Ag need high energy-consumption thermal evaporation process which can be made only with expensive evaporation equipment under vacuum. All the factors elevate the threshold of PVSCs' commercialization. Carbon material, on the other hand, is a readily available electrode candidate for the application as CE in the PVSCs. In this review, endeavors on PVSCs with low-cost carbon materials will be comprehensively discussed based on different device structures and carbon compositions. We believe that the PVSCs with carbon-based CE hold the promise of commercialization of this new technology.

Keywords: perovskite solar cell, counter electrode, carbon material, commercialization

PACS: 88.40.H–, 88.40.hj, 88.40.hm **DOI:** 10.1088/1674-1056/27/1/018805

1. Introduction

Along with the gradual exhaustion of fossil energies and the environmental pollution caused by employing them, people increasingly realize the importance of renewables. Solar energy is the most abundant energy in the world. In order to convert solar energy into electric energy which can be directly used by modern society, various kinds of solar cells were designed. Solar cell technologies are grouped into three generations by Martin Green,[1] the first generation usually refers to mono-crystalline silicon and poly-crystalline silicon solar cells,[2–4] the second generation is the family of thin film solar cells (such as cadmium sulphide, cadmium telluride, copper indium diselenide, and amorphous silicon), and the third generation includes polymer solar cell (PSC), dye-sensitized solar cell (DSSC), quantum dot solar cell (QDSC), and so on, which utilize new materials and nanotechnology. So far, the family of silicon-based solar cells dominates the world's photovoltaic market, but they suffer from drawbacks such as high manufacturing cost, high energy-consumption processes, and severe environmental pollution during the production process. The so-called second generation solar cells, namely, thin-film solar cells, also have some shortcomings, for instance, low power conversion efficiency (PCE), scarcity of raw materials, and operational instability. The third-generation solar cells show great prospect because of their interesting features including low-cost, less energy consumption, and abundant raw materials. Therefore, the third-generation solar cells conform to the trend of the commercial market of the photovoltaic industry.

Among the third-generation solar cells, dye-sensitized solar cells (DSSCs)[5] attracted intensive research interest due to the low-cost materials and ease of fabrication. The upsurge of investigations on perovskite solar cells (PVSCs) sprang from the community of DSSCs. Since the pioneering work of Kojima *et al.* who introduced $CH_3NH_3PbBr_3$ and $CH_3NH_3PbBr_3$ as light absorbers in a liquid-state perovskite-sensitized solar cell in 2009, PVSCs have allured intensive studies both from the academic world and industrial community.[6–9] With thousands of publications and increasing attempts to commercialization, PVSCs gradually become an almost matured technology during the past eight years.[10]

PVSCs usually consist of matrix-supported transparent conductive oxide (TCO) anode, charge selective contact layer (hole/electron transport layer or H(E)TL), perovskite absorbed layer, second charge selective contact layer (electron/hole transport layer), and cathode.[11] PVSCs generate electricity according to the following mechanism (Fig. 1): Once illuminated by sunlight, the perovskite layer would absorb photons which have higher energy than its band gap, and the electron/hole pairs generated in the perovskite layer can be dissociated at the interfaces of perovskite/H(E)TL. Electrons are injected into the conduction band of the ETL and collected by

*Project supported by "Hundred Talents Program" of the Haixi Institute, Chinese Academy of Sciences (Grant No. 1017001) and "Thousand Talents Program" of China.
†Corresponding author. E-mail: peng.gao@fjirsm.ac.cn
© 2018 Chinese Physical Society and IOP Publishing Ltd

the anode, while holes are transported to the valence band of the HTL and compiled by the cathode. Electrons flow through the external circuit and arrive at the cathode where they reunite with holes.[12] Due to the unique semiconducting and conducting properties of the perovskite crystal, such as high optical absorption coefficient, appropriate direct band gap around 1.5 eV, ambipolar charge mobility, long carrier lifetime, and long carrier diffusion length,[13] PVSCs have nowadays obtained a certified efficiency record of 22.1%,[14] which is even higher than that of the commercialized polycrystalline silicon solar cells. However, there are still some issues blocking the way towards the commercialization of PVSCs, for instance, the instability of the perovskite contacts with moisture and oxygen,[15] the high cost of typical hole-transporting-material (HTM) (such as spiro-OMeTAD, P3HT, and PTAA) and noble metallic counter electrode (CE) like gold and silver, the long-time stability of the cell under ambient condition, some high energy-consumption processes of device fabrication, and harsh requirement for fabrication facilities.

Using Au or Ag as the CE is indispensable to fabricate state-of-the-art PVSCs, but Au is too expensive for mass industrial manufacture and evaporating Au or Ag onto the top of the cell is a high energy-consumption process which needs high vacuum and high temperature. Domanski *et al.* found that, when PVSCs are exposed to a temperature of 70 °C, considerable amounts of gold from the back electrode will diffuse across the HTL into the perovskite material, resulting in dramatic loss of the device performance under working conditions.[16] Ag is cheaper and works well in PVSCs with HTM, but it can become corroded when in contact with the perovskite film, which is likely to be due to the formation of silver halide.[17] Hence, replacing the noble metal cathode with low-cost back electrode materials is imperative. Through the unremitting endeavor of many research groups, carbon materials as the cost-efficient choice of back electrodes have been introduced to PVSCs to address issues above. In this review, the application of carbon materials acting as CEs in PVSCs will be exhibited. We will discuss constructions, properties, and morphologies of those materials employed as electrodes, and how these characters affect the performance of the corresponding device. A summary of almost all research works using carbon as counter electrode is shown in Table 1.

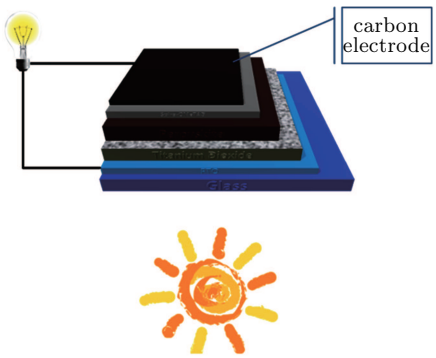


Fig. 1. (color online) The working carbon based PVSC under sunlight.

Table 1. A summary of almost all research works using carbon as counter electrode.

Electrode material	*FF*	V_{OC}/V	J_{SC}/mA·cm^{-2}	PCE/%	Device structure	Method	Ref.
Carbon black/flaky graphite (carbon paste)	0.46	0.825	10.6	4.08	FTO/TiO_2dense layer/mesoporous TiO_2/$CH_3NH_3PbI_3$/ZrO_2space layer/carbon black/graphite	screen printing	[18]
Carbon black/spheroidal graphite (carbon paste)	0.61	0.878	12.4	6.64	FTO/TiO_2dense layer/mesoporous TiO_2/$CH_3NH_3PbI_3$/ZrO_2space layer/carbon black/graphite	screen printing	[18]
Carbon black	0.71	0.95	17.20	11.60	FTO/TiO_2compact layer/$CH_3NH_3PbI_3$/nano carbon	inkjet printing	[19]
Carbon black/graphite (carbon paste)	0.57	0.953	18.73	10.20	FTO/TiO_2 dense layer/TiO_2mesoscopic layer/$CH_3NH_3PbI_3$/ mesoscopic carbon layer/industrial flexible graphite sheet	screen printing	[20]
Commercial carbon paste	0.55	0.90	16.78	8.31	FTO/TiO_2 compact layer/TiO_2mesoscopic layer/$CH_3NH_3PbI_3$/ commercial carbon paste	doctor-blading	[21]
Commercial conductive carbon paste	0.54	0.80	21.02	9.08	FTO/TiO_2 compact layer/TiO_2 mesoscopic layer/$CH_3NH_3PbI_3$/ carbon	doctor-blade coating	[22]
Carbon black/graphite (carbon paste)	0.66	0.858	22.8	12.84	FTO/TiO_2 dense layer/mesoporous TiO_2/$CH_3NH_3PbI_3$/ZrO_2layer/carbon black/graphite	printing	[23]
Carbon black/graphite (carbon paste)	0.61	0.868	20.1	10.64	FTO/TiO_2 dense layer/mesoporous TiO_2/$CH_3NH_3PbI_3$/ZrO_2layer/carbon black/graphite	screen printing	[24]
Carbon black/graphite (carbon paste)	0.76	0.915	21.62	15.03	FTO/TiO_2 compact layer/TiO_2/Al_2O_3/NiO/carbon (a quadruple-layer)/$CH_3NH_3PbI_3$	screen-printing	[25]
Carbon black/graphite (carbon paste)	0.72	0.90	20.45	13.14	FTO/TiO_2 dense layer/mesoporous TiO_2/$CH_3NH_3PbI_3$/ZrO_2layer/carbon black/graphite	screen-printing	[26]
Graphite flake/carbon black powder (carbon paste)	0.63	1.002	21.30	13.53	FTO/TiO_2 dense layer/mesoporous TiO_2/$CH_3NH_3PbI_3$/ thermoplastic carbon film/Al foil	doctor-blading	[27]
Conductive-carbon paste	0.54	0.810	19.98	8.73	FTO/C-ZnO/$CH_3NH_3PbI_3$/carbon	doctor-blading	[28]
conductive-carbon paste	0.42	0.76	13.38	4.29	ITO/PEN/ZnO/$CH_3NH_3PbI_3$/carbon	doctor-blading	[28]
Carbon black/graphite (carbon paste)	0.71	0.89	18.2	11.4	FTO/TiO_2/NiO/$CH_3NH_3PbI_3$/carbon	screen printing	[29]
Commercial carbon paste	0.75	1.03	20.1	15.5	FTO/TiO_2/mp-TiO_2/$CH_3NH_3PbI_3$/doped-TPDI/carbon	doctor-blading	[30]
Carbon black/graphite (carbon paste)	0.76	0.917	21.36	14.9	FTO/TiO_2/mp-TiO_2/$CH_3NH_3PbI_3$/ZrO_2/NiO/carbon black/graphite	blade coating	[31]

Table 1. (*Continued*).

Electrode material	*FF*	V_{OC}/V	J_{SC}/mA·cm^{-2}	PCE/%	Device structure	Method	Ref.
SWCNT doped graphite/carbon black (carbon paste)	0.69	1.01	21.26	14.7	FTO/compact TiO_2/TiO_2 and Al_2O_3 layer/$CH_3NH_3PbI_3$/carbon SWCNTs	printing	[32]
Carbon paste (flake graphite/ graphite powder/ carbon black/ ZrO_2 powder)	0.474	0.97	23.5	10.8	FTO/TiO_2/mp-TiO_2/$CH_3NH_3PbI_3$/carbon/PDMS	doctor-blading	[33]
Carbon black/graphite (carbon paste)	0.572	0.457	19.63	5.13	FTO/TiO_2/mp-TiO_2/$CH_3NH_3Sn_yPb_{1-y}I_{3-x}Cl_x$/ Al_2O_3/carbon	screen-printing	[34]
Carbon paste	0.46	0.843	14.19	5.56	FTO/ZnO dense layer/$CH_3NH_3PbI_3$/(ZnO/TiO_2NR layer)/ZrO_2layer /carbon layer	screen-printing	[35]
Carbon paste	0.58	0.960	14.82	8.23	FTO/ZnO dense layer/$CH_3NH_3PbI_3$/ZnO NR layer/ZrO_2layer/ carbon layer	screen-printing	[35]
Soot of a burning candle	0.42	0.82	12.30	4.24	FTO/TiO_2/mp-TiO_2/$CH_3NH_3PbI_3$/spiro-OMeTAD/carbon/FTO	using FTO glass as substrate to collect soot of a burning candle	[36]
Carbon black/graphite (carbon paste)	0.723	0.846	20.04	12.3	FTO/TiO_2/mp-TiO_2/ $CH_3NH_3PbI_3$/Al_2O_3/carbon	screen-printing	[37]
Low-temperature conductive carbon paste (graphite flake, nanographite powder, and carbon black)	0.44	0.85	18.3	6.88	FTO/TiO_2/mp-TiO_2/$CH_3NH_3PbI_3$/carbon	doctor-blading	[38]
Carbon black/graphite (carbon paste)	0.50	0.81	18.40	7.29	FTO/TiO_2/mp-TiO_2/$CH_3NH_3PbI_3$/carbon	doctor-blading	[39]
Conductive carbon ink	0.60	0.89	21.43	11.44	FTO/TiO_2/mp-TiO_2/$CH_3NH_3PbI_3$/carbon	doctor-blading	[40]
Commercial carbon paste (carbon black, graphite, and epoxy)	0.65	1.04	21.27	14.38	FTO/TiO_2/mp-TiO_2/$CH_3NH_3PbI_3$/carbon	printing	[41]
Insulator cloth embedded in carbon paste	0.429	1.08	18.42	8.70	FTO/TiO_2/mp-TiO_2/perovskite/spiro-OMeTAD/carbon	doctor-blading	[42]
Carbon cloth embedded in carbon paste	0.67	1.12	20.42	15.29	FTO/TiO_2/mp-TiO_2/perovskite/spiro-OMeTAD/carbon	doctor-blading	[42]
Commercial carbon paste (carbon black, graphite)	0.67	1.0	21.83	14.58	FTO/TiO_2/mp-TiO_2/$CH_3NH_3PbI_3$/carbon	paint	[43]
Carbon paste	0.75	0.893	22.43	15.0	FTO/TiO_2/mp-TiO_2/$CH_3NH_3PbI_3$/Al_2O_3/carbon	screen-printing	[44]
Carbon paste	0.667	0.861	16.57	9.53	FTO/TiO_2 compact layer/silver contact/TiO_2 mesoscopic layer/$CH_3NH_3PbI_3$/ZrO_2/carbon	screen-printing	[45]
Carbon paste (carbon black, graphite)	–	–	–	11.07	FTO/TiO_2/mp-TiO_2/$CH_3NH_3PbI_3$/mesoporous ZrO_2/carbon	–	[46]
Boron and phosphorus co-doped carbon	0.61	0.90	12.35	6.78	FTO/TiO_2/mp-TiO_2/$CH_3NH_3PbI_3$/boron and phosphorus co-doped carbon/Al foil	doctor-blading	[47]
Carbon black/graphite (carbon paste)	0.72	0.965	20.4	14.2	FTO/TiO_2/mp-TiO_2/$CH_3NH_3PbI_3$/NiO nanosheets/carbon	screen-printing	[48]
Carbon	0.59	0.857	20.79	10.53	FTO/TiO_2 dense layer/W-doped mesoporous TiO_2/ $CH_3NH_3PbI_3$/carbon	blade coating	[49]
Commercial carbon paste	0.74	1.05	20.8	16.1	FTO/TiO_2/mp-TiO_2/$CH_3NH_3PbI_3$/CuPc nanorods/carbon	doctor-blading	[50]
Carbon slurry	0.67	0.867	22.93	13.41	FTO/TiO_2/mp-TiO_2/ZrO_2/perovskite/carbon	screen-printing	[51]
Graphite/carbon black (carbon paste)	0.78	0.92	19.21	13.89	FTO/TiO_2/mp-TiO_2/ZrO_2/perovskite/carbon	screen printing	[52]
Carbon paste	0.77	0.94	21.45	15.60	FTO/TiO_2/mp-TiO_2/ZrO_2/perovskite/carbon	screen printing	[53]
Commercial carbon paste	0.72	1.35	8.35	8.09	FTO/TiO_2/mp-TiO_2/$CH_3NH_3PbBr_3$/carbon	printing	[54]
Commercial carbon paste (carbon black/ graphite)	0.68	1.29	5.7	5.0	FTO/TiO_2/mp-TiO_2/$CsPbI_3$/carbon	painting	[55]
Graphite	0.644	0.803	20.1	10.4	FTO/TiO_2/mp-TiO_2/perovskite/carbon	doctor-blading	[56]
Commercial carbon paste	0.55	0.97	19.1	10.19	FTO/TiO_2/mp-TiO_2/perovskite/carbon	printing	[57]
Carbon paste	0.65	1.04	21.27	14.38	FTO/ TiO_2/mp-TiO_2/perovskite/carbon	-	[58]
Carbon paste	0.68	0.88	15.10	9.10	FTO/TiO_2/mp-TiO_2/ZrO_2/perovskite($MAPbI_3$)/carbon	screen printing	[59]
Carbon paste	0.74	1.00	19.31	14.35	FTO/TiO_2/mp-TiO_2/ZrO_2/perovskite ($MAPbI_3$·xGuCl)/carbon	screen printing	[59]
Carbon black/graphite (carbon paste)	0.69	1.04	15.37	11.03	FTO/TiO_2/mp-TiO_2/Al_2O_3/perovskite/carbon	screen printing	[60]
Carbon paste	0.76	0.957	18.15	13.24	FTO/TiO_2/mp-TiO_2/$CH_3NH_3PbI_{(3-x)}(BF_4)_x$/$ZrO_2$/carbon	screen-printing	[61]
Candle soot	0.72	0.90	17.00	11.02	FTO/TiO_2/mp-TiO_2/$CH_3NH_3PbI_3$/carbon /FTO	rolling transfer	[62]
Carbon paste	0.66	0.90	20.7	12.30	FTO/TiO_2/mp-TiO_2/ porous Al_2O_3/$CH_3NH_3PbI_3$/carbon	screen printing	[63]
Carbon paste	0.68	0.78	15.1	8.0	FTO/TiO_2/mp-TiO_2/porous Al_2O_3/perovskite/carbon	doctor-blading	[64]
Carbon paste	0.53	1.00	22.67	12.02	FTO/TiO_2/mp-TiO_2/$CH_3NH_3PbI_3$/carbon	doctor-blading	[65]
Laminated carbon nanotube networks	0.51	0.88	15.46	6.87	FTO/TiO_2/mp-TiO_2/$CH_3NH_3PbI_3$/CNT film	transfer	[66]
Carbon nanotubes	0.68	0.99	14.36	8.31	Ti foil/TiO_2 NTs/ $CH_3NH_3PbI_3$/spiro-OMeTAD/carbon nanotubes	transfer	[67]
SWCNT	0.61	1.1	20.3	13.6	FTO/TiO_2/mp-TiO_2/ $(FAPbI_3)_{0.85}(MAPbBr_3)_{0.15}$/ spiro-OMeTAD/SWCNT	press transfer	[68]

Table 1. (*Continued*).

Electrode material	*FF*	V_{OC}/V	J_{SC}/mA·cm^{-2}	PCE/%	Device structure	Method	Ref.
Cross-stacked super-aligned carbon nanotube (CSCNT) sheets with 25-layer CNTs	0.53	0.878	14.43	6.81	FTO/TiO_2/mp-TiO_2/$CH_3NH_3PbI_3$/Al_2O_3/CSCNTs/PMMA	transfer	[69]
CSCNT sheets with 50-layer CNTs	0.68	0.849	14.91	8.60	FTO/TiO_2/mp-TiO_2/$CH_3NH_3PbI_3$/Al_2O_3/CSCNTs/PMMA	transfer	[69]
Iodine doping CSCNT sheets with 50-layer CNTs	0.71	0.853	17.22	10.54	FTO/TiO_2/mp-TiO_2/$CH_3NH_3PbI_3$/Al_2O_3/CSCNTs/PMMA	transfer	[69]
CSCNT sheets with 75-layer CNTs	0.64	0.823	15.81	8.35	FTO/TiO_2/mp-TiO_2/$CH_3NH_3PbI_3$/Al_2O_3/CSCNTs/PMMA	transfer	[69]
Thermally treated CSCNT sheets with 50-layer CNTs	0.69	0.840	16.21	9.37	FTO/TiO_2/mp-TiO_2/$CH_3NH_3PbI_3$/Al_2O_3/CSCNTs/PMMA	transfer	[69]
Multi-walled carbon nanotubes	0.59	0.926	21.3	11.6	FTO/TiO_2 dense layer/(TiO_2/SiO_2 scaffold layer)/$CH_3NH_3PbI_3$/carbon	doctor-blading	[70]
Boron doped multi-walled carbon nanotubes	0.77	0.92	–	15.23	FTO/TiO_2/mp-TiO_2/$CH_3NH_3PbI_3$/Al_2O_3/B-doped MWNT	drop-casting	[71]
Multi-walled carbon nanotube (MWCNT)	0.80	0.88	18.00	12.67	FTO/TiO_2/$CH_3NH_3PbI_3$/MWCNT	drop cast	[72]
NiO/SWNCT	0.64	0.945	20.7	12.7	FTO/TiO_2/mp-TiO_2/Al_2O_3/NiO/SWNCT	screen printing	[73]
Graphene	0.67	0.96	19.17	12.37	FTO/compact-TiO_2/$CH_3NH_3PbI_{3-x}Cl_x$/Spiro-OMeTAD/PEDOT:PSS/graphene/PMMA/PDMS	laminate	[74]
Three-dimensional honeycomb like structured graphene (3DHG)	0.63	0.89	18.11	10.06	FTO/TiO_2/($CH_3NH_3PbI_3$/3DHG)/3DHG	doctor-blading	[75]
Single-layered graphene (SG)	0.54	0.878	14.2	6.7	FTO/TiO_2/perovskite bilayer/SG	spin-coating	[76]
Multilayered grapheme (MG)	0.73	0.943	16.7	11.5	FTO/TiO_2/perovskite bilayer/MG	spin-coating	[76]

2. Carbon materials based counter electrodes

Carbon materials have many merits including abundant sources, low-cost, high electrical conductivity, chemical stability, diversity, and modifiability.[77] The appropriate 5.0 eV work function near to that of Au (5.1 eV) makes carbon an ideal candidate for PVSCs' back electrode. According to the different bonded patterns of carbon atoms and different dimensions of crystalline structures, there are several allotropes with very different chemical and physical properties in the elemental carbon family, such as diamond, graphite, graphene, graphdiyne, C60, carbon nanotube, and amorphous carbon, as shown in Fig. 2.[78]

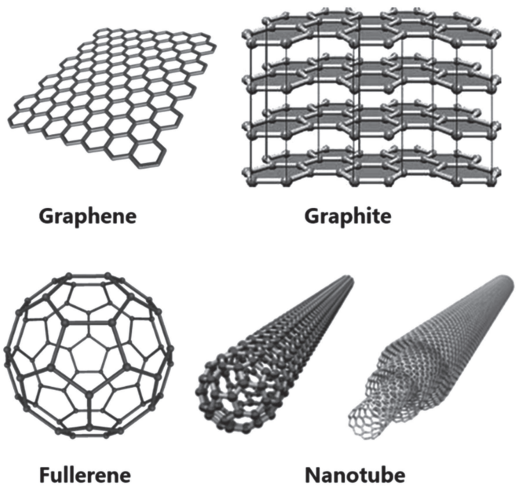


Fig. 2. Structure of various carbon materials.

2.1. Carbon paste

Carbon paste is mainly prepared by graphite and carbon black and is often formed on the top of hole-conductor-free PVSCs. Graphite is a soft, soapy, hexagonal layered crystal with some particular characteristics such as high-temperature resistance, excellent electrical conductivity and thermal conductivity, lubricity, anti-corrosion, plasticity, and thermal shock resistance. Carbon black is a light, loose, and extremely fine black powder produced by incomplete combustion or thermal decomposition of carbon aceous matter under insufficient air condition. Carbon black is one kind of amorphous carbon. The so-called 'amorphous carbon' does not indicate that the shapes of carbon black are confused, but it means the inner turbostratic structure of stacking graphite layers.[78] There are mainly two types of device configurations in carbon CE based PVSCs. One is called the monolithic structure which was previously reported in DSSCs featuring the loading of perovskite in the last step (Fig. 3(a)),[79] and the other one is the conventional structure (Fig. 3(b)) which is

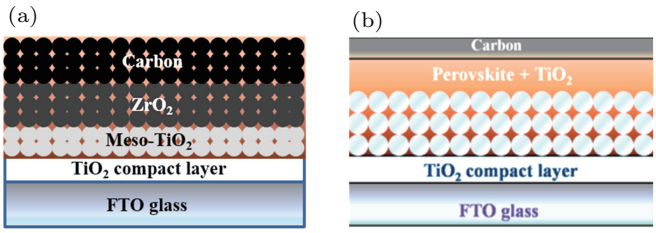


Fig. 3. (color online) Schematic structure of device configurations in carbon CE based PVSCs: (a) monolithic structure; (b) conventional structure. Reprinted from Ref. [21].

fabricated by a layer-by-layer process and a condensed carbon layer atop. In this section, we will discuss carbon paste based CEs used in these two device configurations.

2.1.1. Monolithic structure

In 2013, Hongwei Han's group established a hole-conductor-free $CH_3NH_3PbI_3$ perovskite/TiO_2 heterojunction solar cell which first introduced carbon black/spheroidal graphite as a counter electrode to substitute the noble metallic electrode, and an impressive PCE of exceeding 6.64% was obtained. This carbon black/graphite back electrode was screen-printed on the top of the TiO_2 nanocrystalline layer, then the $CH_3NH_3PbI_3$ precursor was dipped on top of the mesoscopic carbon layer, and finally a device configuration of FTO glass substrate/TiO_2 dense layer/TiO_2 mesoscopic layer/ZrO_2 space layer/carbon layer was formed, which is named monolithic structure.[25,79] The device was fabricated by a simple process like screen printing and showed a long-term stability in the dark after 840 hours. This work initiated the research to low-cost carbon back electrode based PVSCs.[18] Later, they did a series of work on the carbon-based electrode PVSCs.

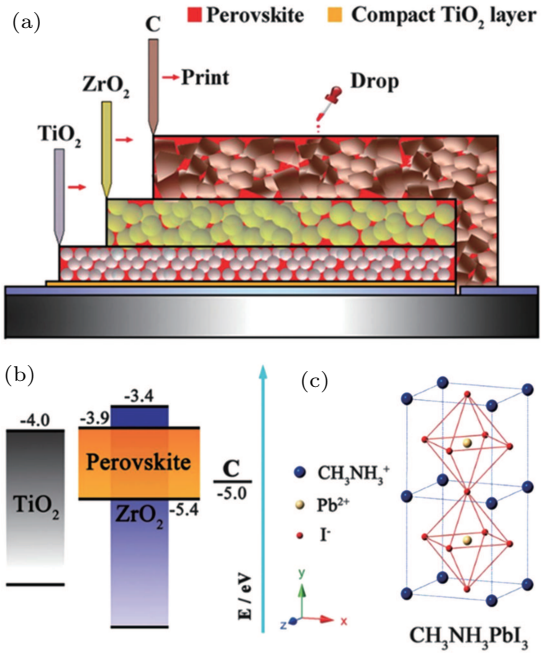


Fig. 4. (color online) (a) The crystal structure of $CH_3NH_3PbI_3$ perovskite and the corresponding energy levels of TiO_2, $CH_3NH_3PbI_3$, and carbon. (b) A schematic structure of the carbon-based monolithic device. Reprinted from Ref. [18].

In 2014, they introduced a mixed-cation perovskite (5-AVA)$_x$(MA)$_{1-x}$PbI$_3$ to replace $MAPbI_3$ in almost the same triple-layer structure of TiO_2/ZrO_2/carbon, as shown in Fig. 4. The 5-AVA molecules formed linear hydrogen-bonded chains between their COOH and NH_3^+ groups and I^- ions from the PbI_6 octahedra, acting as a templating agent to create mixed-cation perovskite (5-AVA)$_x$(MA)$_{1-x}$PbI$_3$ crystals with lower defect concentrations and better pore filling as well as more complete contact with the TiO_2 scaffold, resulting in a longer exciton lifetime and a higher quantum yield for photoinduced charge separation as compared to $MAPbI_3$. The cell achieved a certified PCE of 12.8 % and showed long-time stability ($>$ 1000 h) in ambient air under full sunlight.[23] A mixed anion strategy that makes BF^{4-} substitute for fractional I^- was also employed, showing a PCE enhancement from 10.54% to 13.24% due to more efficient charge transport and suppressed recombination.[61]

It is known that the device performance depends heavily on the quality of the perovskite layer such as morphology, crystallinity, and density of defects. In the case of mesoporous device structures, higher pore filling of perovskites phase is crucial to achieving high-performance monolithic PVSCs, which generally have thick mesoporous films over 10 μm. Thus, they further studied the solvent effect of the perovskite and found that optimized DMF/DMSO (0.93:0.07, v/v) showed a better wettability because of a decent compromise of polarity and viscosity of the solvent. The as-prepared PVSCs hold better perovskite infiltration, the light harvesting ability and charge separation of the perovskite layer were improved, and then the cell devices displayed a PCE of 13.89%.[52] They also employed a versatile additive of guanidinium chloride to improve the morphology of the $CH_3NH_3PbI_3$ perovskite absorber. An improved contact between the perovskite and carbon layer suppressed the recombination reaction in the device, and the open-circuit voltage of the device was significantly enhanced from 0.88 V to 1.02 V, resulting in a PCE up to 14.35%.[59] Besides, NH_4Cl was added to assist the crystallization of the perovskite. A synergy effect of NH_4Cl and moisture on $CH_3NH_3PbI_3$ crystallization provided a facile way to accomplish complete pore-filling of the perovskite absorbers in the mesoporous triple-layer scaffold in printable PVSCs. Correspondingly, the devices achieved a champion efficiency of 15.60% with $J_{SC} =$ 21.45 mA·cm^{-2}, $V_{OC} = 0.94$ V, $FF = 0.77$ and a lifetime of over 130 days in ambient air with relative humidity of 35%.[53] More parameters including the loading amount and morphology of $MAPbI_3$, the temperature of the substrate, and the precursor relative with the quality of perovskite were optimized in the two-step method fabrication process.[26]

Except for the quality of the perovskite itself, they investigated the size effect of bottom TiO_2 nanoparticles on their printed PVSCs. The size of TiO_2 particles affects the infiltration of the precursor and the contact between the perovskite crystal and TiO_2, which influences the charge transfer at the perovskite/TiO_2 interface. The optimized diameter of 25 nm TiO_2 nanoparticles exhibited the best PCE of 13.41%.[51]

The ZrO_2 film is also very important, who separates the TiO_2 film and carbon film, avoiding any direct contact which influences light harvesting and the transfer of photo-generated

charge. They found that the appropriate thickness of the mesoporous ZrO_2 film was around 1 μm, as a result of a compromise between needs of light harvesting by $MAPbI_3$ confined in the spacer layer, the width of the built-in electric field, and the film quality of the spacer layer.[26]

Also, as a pivotal component, graphite decides the porosity and conductivity of back carbon electrode. Different sizes of graphite will cause differences in the filling of PbI_2 and $CH_3NH_3PbI_3$ precursors and also the square resistance of carbon counter electrode, which will finally affect the performance of the devices. So, they investigated the previous topic, and found that the 8 mm graphite-based carbon back electrode has a more significant average pore size, a smaller square resistance, and hence a higher PCE exceeding 11% compared with others. The square resistance of 9 μm thick carbon CEs employing graphite with different sizes was showed in Table 2.[80]

Table 2. The square resistance of 9 μm thick carbon CEs employing graphite with different sizes. Reproduced from Ref. [80].

	8 μm	6 μm	3 μm	500 nm	40 nm
R_{sq}/Ω	11.47	61.21	132.26	56.68	63.01

Besides Han's work, to realize more mechanization of the fabrication devices process, Hashmi *et al.*[45] replaced manual infiltration of perovskite precursor step used in Han's works with inkjet printing in the same device structure of PVSCs (Figs. 5(a) and 5(b)), and the fabricated devices showed a maximum PCE of 9.53% with high stability when subjected to continuous light soaking stability test over a period of 1046 h without any encapsulation. This work demonstrated the capability and potential of inkjet infiltration of perovskite precursor ink for porous triple layered HTM free printed PVSCs and provides an opportunity to fabricate the large-area devices in future.

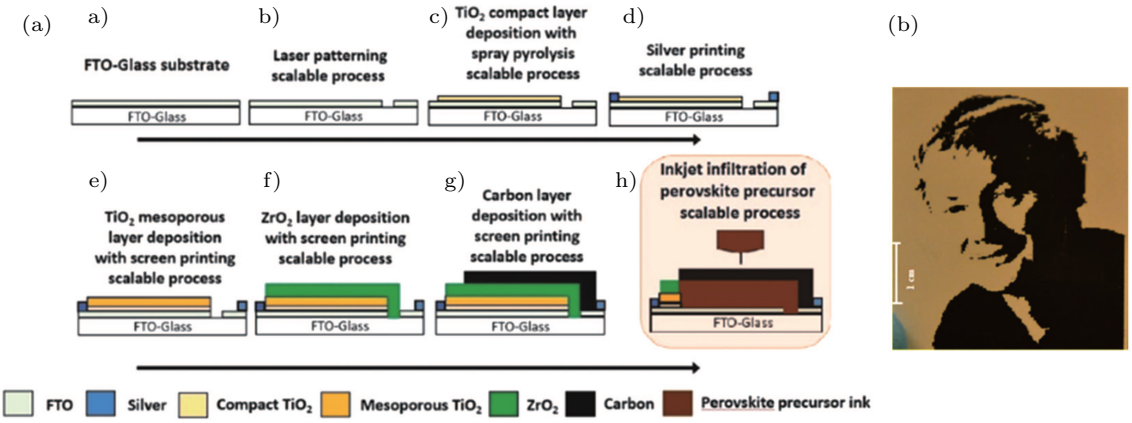


Fig. 5. (color online) (a) Illustration of the scalable process to be employed for the production of HTM free carbon based PVSCs: a) fluorine-doped tin oxide (FTO) coated glass substrate, b) laser patterning of the FTO layer, c) spray pyrolysis for compact TiO_2 layer deposition, d) screen printing of silver contacts, e) screen printing of a mesoporous TiO_2 layer, f) screen printing of an insulating ZrO_2 layer, g) screen printing of a porous carbon composite layer, h) inkjet of a controlled volume of perovskite precursor solution, which is targeted for this work. Note that only scalable processes are highlighted here. The sintering steps consecutive to screen printing are not represented for better clarity. (b) Inkjet printing of bitmap version of a digital image as an example of accurate 2D printing, image reproduced with permission from Alain Herzog/EPFL. Adapted from Ref. [18].

To reduce the interfacial charge recombination, Mingkui Wang's group developed a quadruple layer of $TiO_2/Al_2O_3/NiO$/carbon as scaffold infiltrated with $MAPbI_3$, as shown in Fig. 6. The insulating Al_2O_3 acts as a spacer layer, while the n-type TiO_2 and p-type NiO act as selective contacts for the extraction of electrons and holes, respectively. The $TiO_2/Al_2O_3/NiO$/carbon structured device showed a short-circuit current density (J_{SC}) of 21.62 mA/cm^2, a fill factor (FF) of 0.76, an open-circuit voltage (V_{OC}) of 915 mV, achieving a PCE of 15.03%. For comparison, the device with a configuration of TiO_2/Al_2O_3/carbon ($MAPbI_3$) was also fabricated, showing a lower PCE performance of 11.2% (J_{SC} = 17.59 mA/cm^2, FF = 0.71, and V_{OC} = 896 mV). Incident photon to current conversion efficiency (IPCE) curves of these two kinds of devices were measured, the $TiO_2/Al_2O_3/NiO$/carbon ($MAPbI_3$) device reached a higher value than the TiO_2/Al_2O_3/carbon ($MAPbI_3$) device in the wavelength range of 350–750 nm. The augmented ΔIPCE in the blue region corresponds to carriers generated by high-energy photons in the front section close to the FTO side, indicating that these charges would be efficiently collected when the NiO layer was inserted, most probably due to the direct separation of the electron/hole pair at this interface without having to diffuse through the perovskite itself. Although no organic hole-transport layer was employed to collect holes, a high FF of 0.76 was still observed for the $TiO_2/Al_2O_3/NiO$/carbon ($MAPbI_3$) device. The high FF and IPCE values indicate that the charge transport and collection are very efficient in this device architecture.[25]

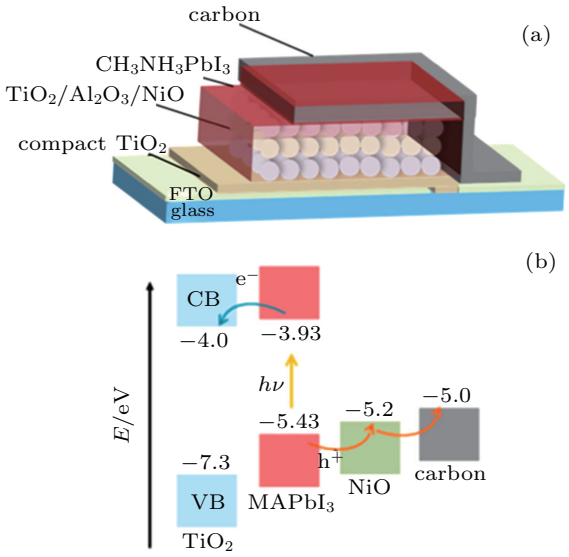


Fig. 6. (color online) Optimized device structure. (a) Schematic representation of the $TiO_2/Al_2O_3/NiO$/carbon ($MAPbI_3$) based device. (b) Energy band diagram of the fabricated device configuration. Reprinted from Ref. [25].

The perovskites adopted in works mentioned above are all organic–inorganic hybrid perovskites. Recently, inorganic perovskites (e.g., $CsPbI_3$, $CsPbBr_3$) attracted extensive attention due to higher stability.[81–83] A printed HTM-free PVSC with all the components made of inorganic materials (porous metal oxide, inorganic perovskite, and carbon) with monolithic configuration showed increased thermal stability. Li *et al.*[84] fabricated lead-free inorganic perovskites $CsSnX_3$-based PVSCs with the structure of FTO/TiO_2/Al_2O_3/$CsSnX_3$/C, the as-prepared all-inorganic devices showed superior thermal stability up to 200 °C, with an average PCE of 3.0% and long-term stability for 77 days without efficiency-loss.

In all the works above, the monolithic PVSCs were usually fabricated by the inexpensive and straightforward screen-printing method, of which the structure avoids costly and unstable organic HTMs and noble metal electrode like Au. These HTM-free carbon-based PVSCs boost the promise of PVSC to commercialization. The monolithic PVSCs have the advantages of ambient condition process, efficacious use of precursor, thick perovskite layer for higher stability, and better contact between perovskite and CE. Meanwhile, the thick metal oxide layers bring disadvantages like the high-temperature process and large series resistance, etc.

2.1.2. Conventional structure

Regarding the carbon paste mentioned above, high-temperature sintering above 400 °C is necessary, which will hamper the large-scale commercialization of carbon-based PVSCs. So, it needs to develop the low-temperature processed CE. Apart from the lower energy consumption, low-temperature (< 150 °C) permits not only to make electrodes straight on top of the perovskites but also to prepare flexible devices. For example, it is possible to print carbon pastes directly on perovskite layers like deposition of Au on top of the perovskites or HTM (e.g., spiro-OMeTAD) in a conventional PVSC. In 2014, Licheng Sun's group first reported a low-temperature-processed commercial carbon paste (100 °C) by doctor blading technology. They deposited the carbon electrode on the two-step method prepared perovskites. Under optimized conditions, the hole-conductor-free perovskite/TiO_2 heterojunction solar cells obtained an impressive PCE of 8.31% and furthermore exhibited excellent stability over 800 h.[21] The structure of perovskite would be destroyed by some solvents in commercial carbon paste which is directly processed on the top of the perovskite film. Thus, Tingli Ma's Group[85] modified the commercial conductive carbon paste with only chlorobenzene as a solvent and obtained an improved PCE of 9.08%.

At almost the same time, Yang's group reported clamping solar cells using candle soot for hole-extraction. In the fabrication process, the perovskite film is fabricated by depositing a PbI_2 precursor layer, immediately followed by the rolling transfer of candle soot, and finally subjecting the sample to a CH_3NH_3I bath treatment, as shown in Figs. 7(a)–7(c). Notably, the hole-extraction rate of candle soot is even comparable with that of traditional spiro-OMeTAD, which was demonstrated by the femtosecond time-resolved photoluminescence (fs-TRPL). The best devices achieved a PCE of 11.02%.[62] Later, they developed an inkjet printing technology to fabricate carbon electrodes in planar TiO_2 based PVSCs. The fabrication process is diagrammatized in Fig. 7(d). By employing the carbon/CH_3NH_3I ink formulation to transform PbI_2 *in situ* to $CH_3NH_3PbI_3$, a reinforced interpenetrating interface between the $CH_3NH_3PbI_3$ and carbon electrodes was formed in comparison with that using pure carbon ink. With minimal charge recombination, a reasonably high PCE of 11.60% was achieved.[19] This type of device processing combined the procedures from monolithic and conventional devices. Their strategy of *in-situ* preparation of perovskite builds an excellent contact between perovskite and CEs, which could avoid the possible adverse effect of carbon paste solvent. However, this method exists apparent defects where their J_{SC} is as low as only 17 mA·cm^{-2}, which might be ascribed to the thin perovskite layer produced by the two-step transformation reaction (PbI_2 layer to perovskite) and always along with unreacted PbI_2.

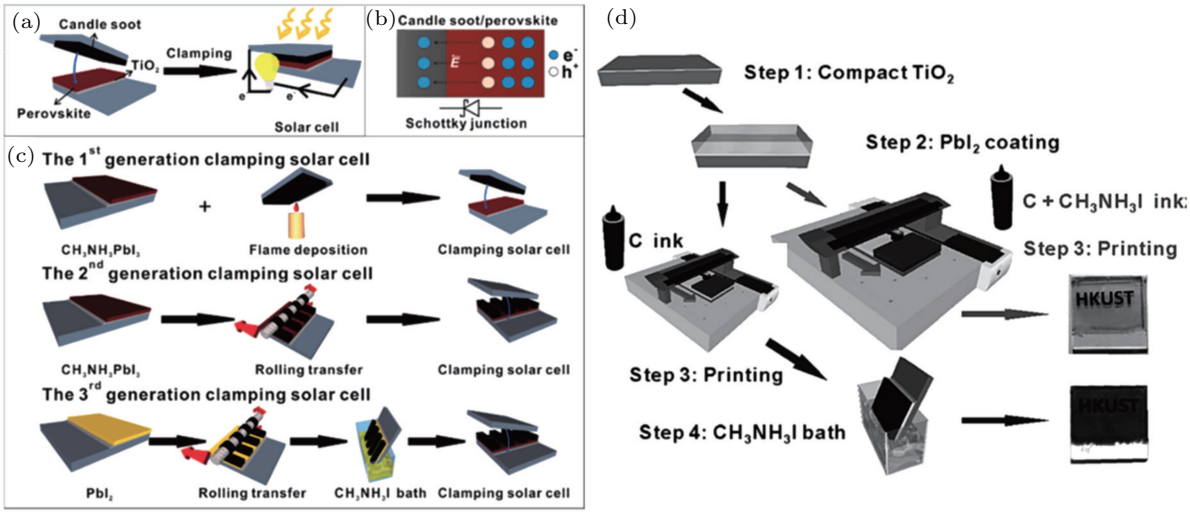


Fig. 7. (color online) (a)–(c) Development of a candle soot/perovskite clamping solar cell. Reprinted from Ref. [62]. (d) Fabrication process flow for the instant inkjet printing of the C/$CH_3NH_3PbI_3$ planar perovskite solar cells. For comparison, a different strategy was used to convert PbI_2 into $CH_3NH_3PbI_3$ using separate step 3 and step 4. Reprinted from Ref. [19].

Then, Yang's group moved efforts towards the fabrication of high-quality perovskites by painting carbon pastes on the top of pre-prepared perovskites. They developed an electrodeposition technique to synthesize the perovskite layer. The electrodeposited perovskite layer was printed with the carbon paint as back contact. The corresponding devices achieved a PCE of 10.19%, and showed an encouraging PCE in a larger cell area up to 4 cm^2.[57] Although the efficiency of the painted carbon-based-PVSCs has come up to over 10%, it is still low compared with the traditional PVSCs with Au or Ag CEs. The primary limiting factor of the efficiency of the painted-carbon-based PVSC lies in the poor contact at the perovskite/carbon interface due to the lamella feature of graphite layer and ease of producing interspace between the graphite flakes and perovskites.[20]

To improve the contact at the perovskite/carbon interface, Yang *et al.* designed a solvent engineering strategy based on two-step sequential method which is beneficial to an excellent pore-filling perovskite layer in a relatively thick mesoscopic TiO_2 scaffold. The solvent for CH_3NH_3I solution at the second step is a mixed solvent of IPA/cyclohexane. This mixed solvent results in a high-quality perovskite layer with smooth surface and compact capping layer which could enhance the contact with CE for a majority of graphite flake in carbon paste. Finally, they obtained the highest PCE of 14.38% with an *FF* of 0.65 and a PCE of 10% for the 1 cm^2 area device.[41] Moreover, through colloidal engineering to form an ultra-even perovskite layer, they boosted the efficiency of the carbon-based PVSCs to 14.58%.[43]

In the presence of high-quality perovskite layer, Sun *et al.* introduced CuPc nanorods as hole-transporting materials to improve the interface contact. The device displayed an impressive PCE of 16.1%, which is comparable to that of the corresponding devices with the doped spiro-OMeTAD as HTMs and noble metal Au as back electrode. CuPc nanorods induce an intimate, large interfacial-area contact with the $MAPbI_3$ crystal grains and carbon counter electrode, therefore leading to a significant enhancement in hole-extraction, and a decrease of charge recombination (Fig. 8).[50] However, the CuPc nanorods were prepared by thermal deposition that needs high-vacuum condition.

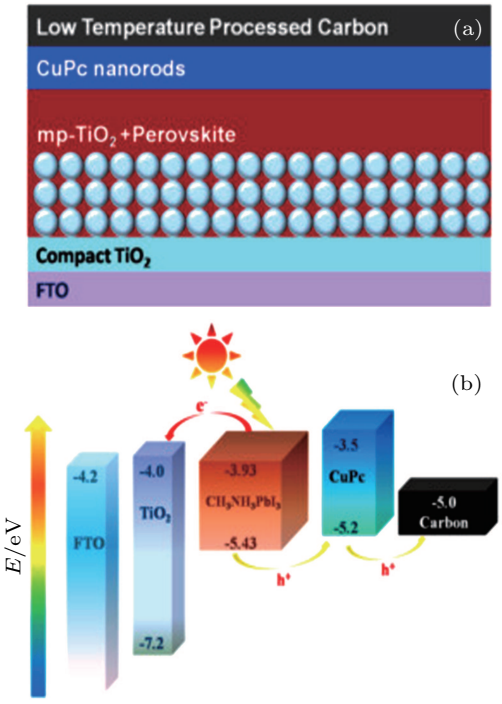


Fig. 8. (color online) Device structure and energy-level diagram: (a) schematics of the whole device: FTO glass/compact TiO_2 layer/mesoporous TiO_2/$CH_3NH_3PbI_3$ capping layer/CuPc/carbon and (b) the corresponding energy level diagram. Fabrication process flow for the instant inkjet printing of the C/$CH_3NH_3PbI_3$ planar perovskite solar cells. For comparison, a different strategy was used to convert PbI_2 into $CH_3NH_3PbI_3$ using separate step 3 and step 4. Reprinted from Ref. [50].

2.1.3. Device engineering on carbon CEs in conventional structure

To enhance the contact of CE and perovskite layer for the favorable charge transport, Qingbo Meng's group developed two-step processed carbon CEs with different graphite flake sizes and contents of carbon black. Firstly, viscous carbon pastes were first coated on the top of the as-prepared devices. Then, a piece of graphite paper was pressed on the carbon paste as an extraction electrode, as shown in Fig. 9. The electrochemical impedance spectroscopy (EIS) of the different cells with carbon CEs was measured to study the charge transport properties. With the lowest charge transfer resistance (R_{CT}) level, the graphite/carbon black composite based cell exhibited a best PCE of 10.2% and a highest FF of 0.572, which suggested that the placid undulation at the surface of smaller graphite flakes, and together with the carbon black particles filling in the interspace, creates more contact sites with the perovskite layer than other cells without doping with carbon black.[20]

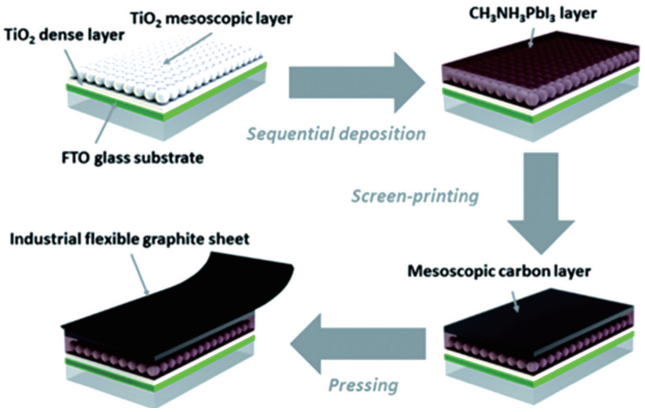


Fig. 9. (color online) Scheme of the fabrication process of all-carbon flexible CE based HTM-free perovskite solar cells. Reprinted from Ref. [20].

Meng *et al.* also fabricated a free-standing flexible carbon electrode containing 20 wt.% polyvinyl acetates (PVAc) in the carbon film to avoid the adverse effect of solvents in carbon pastes. Carbon paste was coated on Teflon film by doctor-blading to form the carbon film after the solvent evaporation. Due to the thermoplastic PVAc, the carbon films can be directly hot-pressed onto the surface of perovskite at 85 °C. With the optimized carbon film components (graphite flakes and carbon black particles with a weight ratio of 3:1 and hot-press pressure 0.25 MPa), champion PCE of 13.53% with an average PCE of 12.03% has been achieved. Compared to PVSCs with Au electrode, this low-cost and stable carbon-based one with low-temperature-processed and flexible carbon counter electrode is promising.[27]

A low-cost carbon cloth embedded in carbon paste as CE was studied by Hagfeldt *et al.*, as shown in Fig. 10(a). When compared to an insulating fiber embedded in carbon paste, the carbon cloth composite obtained an enormous increase in FF. These results showed that the carbon cloth is essential for achieving high-efficiency carbon devices. By a press-transfer process of carbon microfibers in carbon paste, high J_{SC} of 20.4 mA·cm^{-2} and high V_{OC} of 1.12 V were achieved. Moreover, a champion stabilized PCE of 14.8% was achieved.[42]

Additionally, Liao *et al.* reported low-temperature carbon CE based HTM-free mesoscopic PVSCs and encapsulated them by PDMS, as shown in Fig. 10(b). The introduction of PDMS can condense the mesoscopic carbon layer and improve the $MAPbI_3$/carbon interface condition during the solidification of PDMS. Finally, an optimal PCE of 10.8% was achieved. The results exhibit a remarkable 54% enhancement over those without encapsulation (a PCE of 6.88%). The improved performance can be attributed to efficient charge transfer process and slower charge recombination between interfaces. Also, the PDMS layer can isolate moisture in the air, avoiding the degradation of the perovskite. The encapsulated cells show dramatic stability over 3000 hours.[33]

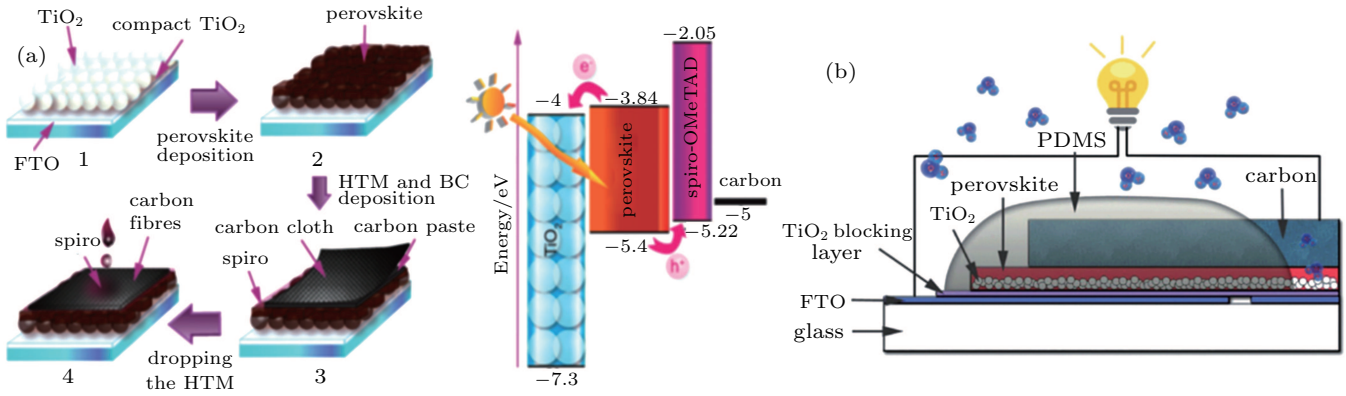


Fig. 10. (color online) (a) a) A schematic image of the carbon cloth/spiro-OMeTAD perovskite solar cell fabrication. b) Energy band alignment of a carbon cloth-based device. Reprinted from Ref. [42]. (b) Schematic representation of the packaged device. Reprinted from Ref. [33].

2.2. Carbon nanotubes

Carbon nanotubes, also called buckytube, have a particular 1D hollow tubular structure, which were uncovered by Iijima in 1991.[86] The tubular structure of CNTs can be considered as the result of rolling up monolayer graphite sheet, so CNTs inherit the admirable properties of graphite such as anti-corrosion, impact resistance, thermal and electrical conductivity.[87] Over the past twenty years, CNTs have attracted researchers majoring in the field of electronic and optoelectronic applications due to their exceptional charge transport property, inherent hydrophobicity, chemical and mechanical stability. CNTs have been incorporated into organic solar cells as electron acceptor successfully. Moreover, the p-type CNTs junctures with n-type silicon were demonstrated to achieve a decent PCE up to 17.0%.[88]

As we know, charge selective contacts on both sides of the perovskite absorbers are crucial elements controlling the whole performance of PVSCs. The inherent p-type nature of CNTs and the decent employment as HTM in organic solar cells make CNTs an alternative HTM for PVSCs. One advantage of using CNTs as HTM is eliminating dopants like lithium salts which are blaming to endanger the long-term stability of PVSCs.[87] Also, the mechanical resilience of CNTs may prove to be particularly beneficial for the development of flexible perovskite solar cells. In this section, some significant efforts introducing CNTs into PVSCs acting as hole conductor and extraction counter electrode will be presented.

Jang *et al.* developed a dripping method to drip multi-walled carbon nanotubes (MWCNTs)/chlorobenzene solution on perovskite precursor solution at the time of its spinning, as shown in Fig. 11. The device completed by screen printing carbon paste as counter electrode exhibited a superior efficiency of 13.57% with almost hysteresis-free performance. Compared to cells fabricated by directly spin-coating CNTs on the as-prepared perovskite layer (referred to herein as post-CNT), the CNT dripping method played a significant role in enhancing the performance of the PVSCs. Under this modified solvent engineering, CNTs were efficaciously inserted into the grain boundaries of the perovskite to create a CNT-perovskite heterojunction. The CNTs shaped motorways for fast hole extraction towards carbon electrode, boosting the J_{SC} value of the devices. Also, the contact at the perovskite/carbon interface was enhanced by the CNTs, as is proved by the lessened series resistance (R_S) and charge transfer resistance (R_h) shown in Table 3.[89] Additionally, the moisture stability was also enhanced by CNT dripping. For the stability test, the as-prepared devices without encapsulation were exposed at 30 °C under 50% humidity for the first two hours and 80% humidity for the next two hours, and the referenced PVSCs employing spiro-OMeTAD as HTM and Au as electrode were tested under the same conditions. The results revealed that the device with CNT modified carbon paste as electrode showed high moisture stability even at 80% RH, retaining 90% initial PCE after the test. By contrast, the reference device lost nearly 80% of the original PCE. The author pointed out that the hydrophobic property of the carbon prevented water from permeating into the devices, which is the typical reason for the perovskite degradation. Moreover, in the reference PVSCs, the spiro-OMeTAD as HTM needs to be doped with Li-bis(trifluoromethanesulfonyl)-imide (Li-TFSI) due to poor conductivity of the pristine film. Nevertheless, Li-TFSI is hygroscopic, which is vulnerable to moisture and can accelerate degradation of the perovskite.

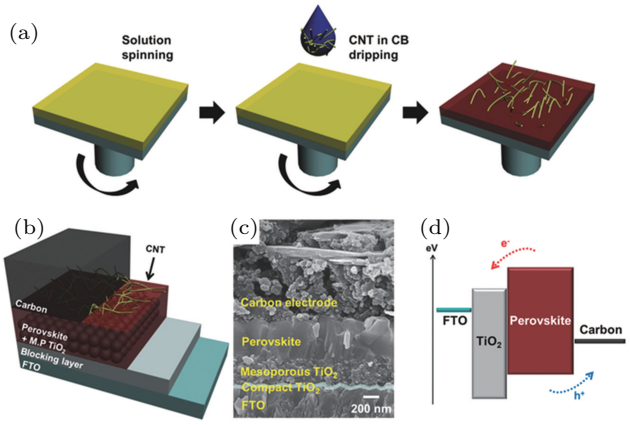


Fig. 11. (color online) Schematic illustrations of (a) the perovskite layer deposition procedure and (b) the prepared carbon electrode-based perovskite solar cells. (c) A cross-sectional SEM image of the prepared device. (d) An energy diagram of the materials used in this work. Reprinted from Ref. [89].

Table 3. Summary of resistances of devices with a perovskite layer fabricated under various conditions. Adapted with permission from Ref. [89].

Sample	R_S/Ω	R_h/Ω
CNT-dripping	19.04	212.46
Post-CNT	23.01	263.97

Different from Jang's work that dripping CNTs into the perovskite layer, Mingkui Wang *et al.* designed single-walled carbon nanotubes (SWCNTs)/carbon composite counters electrodes by printing carbon paste on the top of the Al_2O_3 layer and formed a triple layer structure of $TiO_2/Al_2O_3/C$, as shown in Figs. 12(a) and 12(b). This carbon paste was prepared by dissolving SWCNTs, ZrO_2, carbon black, and graphite into ethyl alcohol. Efficiency up to 14.7% was achieved for a device containing 0.05 wt.% SWCNTs in CE with a V_{OC} of about 1.01 V, a J_{SC} of 21.26 mA/cm^2, and an FF of 0.69. Under the same conditions, a device without SWCNTs in the CE displayed a PCE of 9.9% with a V_{OC} of 0.889 V, a J_{SC} of 20.26 mA·cm^{-2}, and an FF of 0.55. Adding SWCNTs in the carbon counter electrode modifies their working function and prolongs the charge recombination lifetime as well. Both are advantageous to the device performance, especially the output photovoltage and FF.[32]

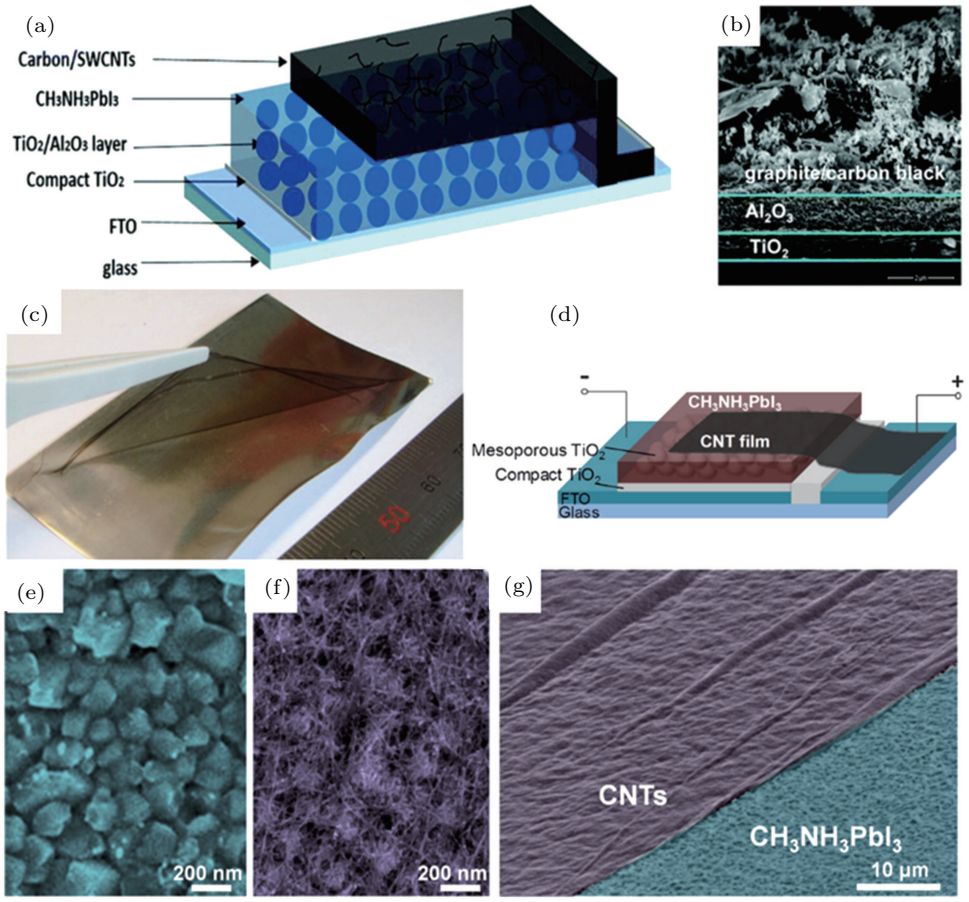


Fig. 12. (color online) (a) Schematic architecture of the investigated device consisting of FTO as a transparent substrate, a compact TiO_2 layer, a mesoporous TiO_2 layer, an Al_2O_3 layer coated with SWCNT added graphite/carbon black CE, (b) cross-section SEM image of a mesoscopic perovskite solar cell. Reprinted from Ref. [32]. (c) Photo of freestanding CNT film lifted by tweezers to transfer onto other substrates. (d) Schematic of $CH_3NH_3PbI_3$ perovskite solar cell with CNT film electrode. (e) Top view SEM images of $CH_3NH_3PbI_3$ perovskite substrate before and (f) after CNT transfer. (g) Tilted SEM image of $CH_3NH_3PbI_3$ perovskite substrate (blue) partly covered by CNT film (purple). Reprinted from Ref. [66].

One of the initial works that employ CNTs as hole conductor in mesoscopic PVSCs was made by Mhaisalkar *et al.* in 2014.[66] In this work, PVSCs were fabricated by laminating freestanding films of CNTs network atop the perovskite absorbers, as shown in Figs. 12(c)–12(g). The network films were synthesized by the floating-catalyst-chemical-vapor-deposition method and then transferred to the as-prepared device easily. It is interesting to note that the CNT film showed a dual-function as both hole-transporter and electrode, thus eliminating the need for a metal electrode. The $CH_3NH_3PbI_3$/CNTs perovskite solar cell without conventional HTM and metal electrode achieved a power conversion efficiency of 6.87% under AM 1.5, 100 mW/cm^2 conditions. By adding spiro-OMeTAD to form a composite electrode, the efficiency of this device can be further improved to 9.90% due to the enhanced hole-extraction and reduced charge recombination. With the merits of low cost, a facile fabrication process without a vacuum environment, chemical stability, and electrical compatibility to perovskite, CNTs are potential to replace expensive metal electrodes in PVSCs. Besides, the flexible and transparent CNT film electrodes show great potential in flexible or tandem PVSCs.

Inspired by the work of Mhaisalkar *et al.*, Wong's group used Ti foil as substrate and TiO_2 nanotube arrays as ETM to fabricate flexible PVSCs. In Ti foil-based PVSCs, the non-transparent Ti foil impedes the light incidence from the anode, so the device will not operate if using a metallic counter electrode. Therefore, a CNTs network the same as that of Mhaisalkar *et al.* was introduced as the counter electrode. With 25 μm Ti foil and $TiCl_4$ treatment to the TiO_2 nanotube arrays, a decent efficiency up to 8.31% has been achieved. These cells showed little deterioration to the device performance after 100 mechanical bending cycles, indicating their excellent flexibility.[67]

Among the family of PVSCs, the clan of carbon-based HTM-free is the most promising for commercialization because of its low-cost and superior long-term stability. However, the FF is lower than that of conventional metal-based PVSCs because of the poor contact at the interface of perovskite/carbon. To address the problem of low FF which may hinder the way of commercialization, Shihe Yang's group used MWCNT as a hole-selective counter electrode to replace con-

ventional small organic molecule HTM and metallic electrode. With the drop-casting method, graphite, carbon black, and MWCNT electrodes were fabricated on the same as-prepared substrates. The performance of three as-fabricated carbon-based PVSCs was demonstrated by the different parameters in Table 4. The SEM images of the devices demonstrated the existence of the gaps in the interface of graphite/perovskite and the cracks on the carbon black thin film. Nevertheless, the MWCNT not only formed a consecutive and crack-free thin film but attached onto the perovskite layer tightly with chemical embedment technique, as shown in Figs. 13(a)–13(f). The morphologies significantly control the contact quality of carbon materials and perovskite layer and impact the device performance. Moreover, the negligible hysteresis effect of the MWCNT-based device compared to the other two was attributed to the excellent interface quality of carbon /perovskite and the matching fast hole-extraction. After optimizing the thickness of the PbI_2 precursor layer and MWCNT layer, an hysteresis-free efficiency of 12.67% with a very extraordinarily attractive FF of 0.80 was achieved.[72]

Table 4. Solar cell parameters of the three as-fabricated carbon-based PVSCs. Reprinted from Ref. [72].

Solar cells	V_{OC}/V	J_{SC}/mA·cm^{-2}	FF	PCE/%
Carbon black	0.90	15.98	0.65	9.35
MNCNT	0.88	15.60	0.75	10.30
Graphite	0.93	10.30	0.64	6.13

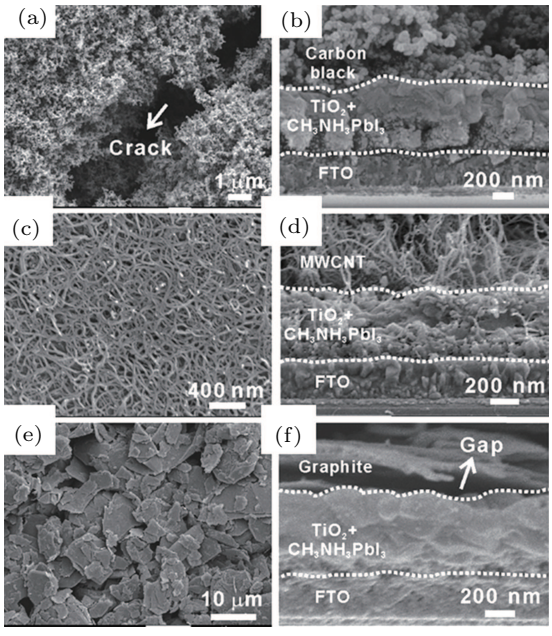


Fig. 13. (a), (c), (e) Top view and (b), (d), (f) cross-sectional SEM images of the carbon black, MWCNT, and graphite-based PVSCs. The dashed lines represent the interface of FTO/TiO_2 and $CH_3NH_3PbI_3$/C, respectively. Reprinted from Ref. [72].

After this, Yang *et al.* boosted their work by doping boron (B) into the MNCNTs, which increases the work function, carrier concentration, and conductivity of the MWCNTs and enhances their ability of hole-extraction and transport. Also, an insulating aluminum oxide (Al_2O_3) thin layer was coated on the mesoporous TiO_2 film as a physical barrier to reduce the charge losses sharply. Finally, the efficiency was promoted to 15.23%.[71] In another case, Hong Lin *et al.* integrated a highly conductive and porous cross-stacked super-aligned carbon nanotube (CSCNT) sheet as a metal-free back contact at low temperature in HTM-free mesoscopic PVSCs, as shown in Fig. 14. The device manufactured with manually transferred CSCNT sheets containing 50-layer CNTs (CSCNT-50) presented a PCE of 8.65% due to its three-dimensional hole-extraction and collection. By doping the CSCNT-50 with iodine (I-CSCNT), the PCE was boosted to 10.54% due to the considerable improvement in the FF and J_{SC} because of the increased grain size and improved crystallinity of perovskite as well as the enhanced conductivity of the I-CSCNT electrode.[69]

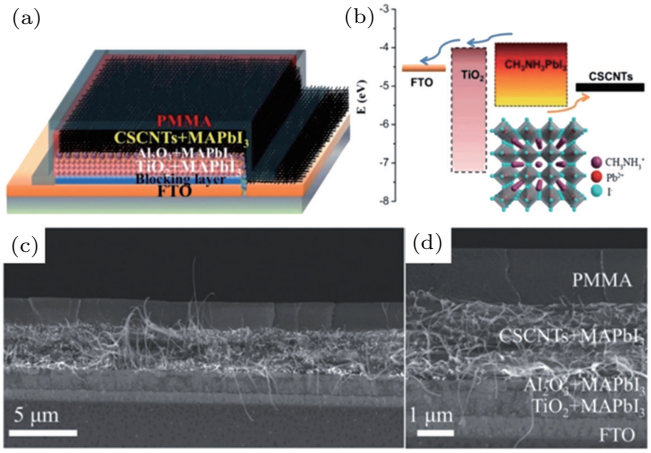


Fig. 14. (color online) (a) Device architecture of the PVSCs tested in this study; (b) the corresponding energy levels of TiO_2, $CH_3NH_3PbI_3$, and CSCNTs; (c) and (d) the cross-sectional SEM images of the typical CSCNT-based PVSCs with different magnifications. Reprinted from Ref. [69].

The overall poor long-term thermal stability is a serious problem that hinders the commercialization of PVSCs. Under elevated temperature condition, considerable amounts of Au from the electrode diffuse across the HTM into the perovskite layer and cause a dramatic loss of the device performance.[16] Aitola *et al.* designed a low-cost CNT-based high temperature-stable PVSC with a configuration of FTO/compact TiO_2/mesoporous TiO_2/perovskite/SWCNT-spiro-OMeTAD, as shown in Fig. 15. The SWCNT solar cells were prepared by cutting the SWCNT film on a filter paper to an appropriate size piece and transferred atop perovskite with some pressure. The SWCNT film was densified with a small amount of chlorobenzene. After that, another SWCNT film was transferred to the first film. The procedure was completed by drop casting spiro-OMeTAD solution on the SWCNT film. Au-based device with a PCE of 18.4% and SWCNT-based device with a PCE of 15.0% were put under the stability testing. During the stability test with a temperature of 60 °C in the

N_2 atmosphere and one sun equivalent white LED illumination, the devices showed only the modest linear efficiency loss, which led to an estimated lifetime of 580 h. For comparison, the standard PCSs with Au electrode exhibited a significant and quick efficiency loss mainly due to the ion migration of gold in the structure.[90]

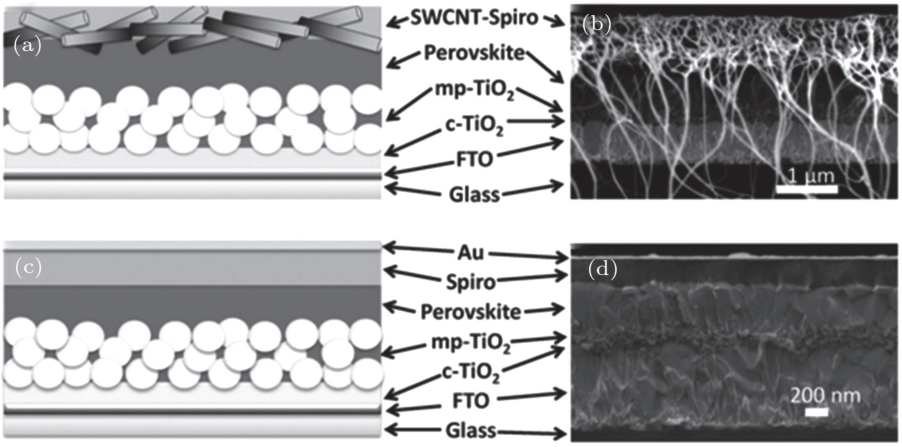


Fig. 15. (a) Schematics and (b) cross-sectional SEM image of the SWCNT-contacted device. The carbon nanotube "whiskers" in front of the SEM image are due to sample preparation. (c) Schematics and (d) cross-sectional SEM image of the standard Au contacted device with spin-coated spiro-OMeTAD HTM. Reprinted from Ref. [90].

2.3. Graphene

In 2004, Novoselov *et al.* successfully prepared a monolayer graphene for the first time by mechanical exfoliation.[91] Since then, graphene has attracted numerous researchers in the field of chemical and material science due to its topping mobility, absorbance, conductivity, mechanical flexibility, transparency, and specific surface area. Now graphene has played more and more important roles in solar cells, energy storage, optoelectronics, electrics, and sensing.[92–95] The first work of graphene-based PVSCs was reported by Snaith *et al.* who utilized nanocomposites of graphene and TiO_2 nanoparticles as the ETM in PVSCs.[96] One significant application for graphene in PVSCs is as bottom electrodes which may replace conventional ITO or FTO transparent electrodes due to its high conductivity, transparency, charge mobility, chemical and mechanical robustness.[97–99] Also, several studies that introduce graphene and its derivatives as PVSCs' HTM have been carried out.[65,100–106] Researchers found that perovskite grown on graphene oxide presents a higher orientation order than that on PEDOT: PSS, as affirmed by XRD measurement.[100] Another group found that the use of reduced graphene oxide HTMs with the inherent passivation-ability markedly prolonged the device lifetime compared to that of PEDOT: PSS based device.[101] Interestingly, Nouri *et al.* designed graphene oxide as HTM and Li-modified graphene oxide as ETM in PVSCs.[65]

In a word, graphene, a magical material, has given rise to many studies in PVSCs. In this paper, we focus on its role as a counter electrode. PVSCs have been exploited for their application in making transparent or semitransparent devices that can absorb light from both sides for the past few years. Those devices can be applied to the building-integrated photovoltaic system, wearable electronics, and tandem cells. The selections of transparent top electrodes are crucial to the performance of the cells. Different electrodes, such as Au,[107–109] Ni,[110] and CNTs,[66] have been studied for their performance in these semitransparent PVSCs. A desired transparent electrode should possess outstanding properties, for instance, high transparency, high conductivity, chemical stability, low cost, and charge collecting ability. Due to its excellent optical and electrical properties, graphene stands out to be an ideal candidate as a transparent electrode in PVSCs. Feng Yan *et al.* reported a semitransparent PVSC by laminating stacked multilayer graphene prepared by the chemical vapor deposition (CVD) method as top transparent electrodes, as showed in Fig. 16(a). The graphene electrodes were fabricated and transferred on flexible plastic substrates and then laminated on perovskite active layers at low temperature (≈ 60 °C) under pressure, which is a facile technique compatible with printing and roll-to-roll processing. The sheet resistance of multilayer graphene will decrease when the number of graphene layers increases and contacts with the PEDOT: PSS layer. After optimizing the electrode's conductivity and its contact with HTM, the double-layer graphene electrodes based devices showed the average PCEs up to 12.02% and 11.65% when the devices were illuminated from the bottom (FTO side) and top (graphene side) electrodes, respectively.[111]

Yang *et al.* employed flexible reduced graphene oxide to synthesize single-layered graphene (SG) and multilayered graphene (MG) as hole-extraction electrodes, as shown in Figs. 16(c) and 16(d). Ultraviolet photoelectron spectroscopy (UPS) was used to check the work functions (Fermi level) of the SG and MG materials. The Fermi levels of MG and SG were determined at -5.0 eV (similar to graphite) and -4.8 eV, respectively. MG collects the merits

of graphite (work function) and monolayer graphene (flexible and spreadable), permitting facile fabrication and energy level engineering simultaneously. Intensity modulated photocurrent/photovoltage spectroscopy (IMPS/IMVS), steady-state photoluminescence (PL), and femtosecond time-resolved photoluminescence (TRPL) revealed that MG-based PVSCs have less recombination and better hole extraction capability than SG-based PVSCs. Indeed, a hole-extraction rate up to 5.1 ns^{-1} measured for MG is comparable to spiro-OMeTAD HTM. Moreover, a Schottky junction was formed in the interface of perovskite/MG, which would accelerate hole-extraction and electron rejection from perovskite. Finally, a decent PCE of 11.5% with a relatively high FF of 0.73 was achieved by using the MG top electrode.[76]

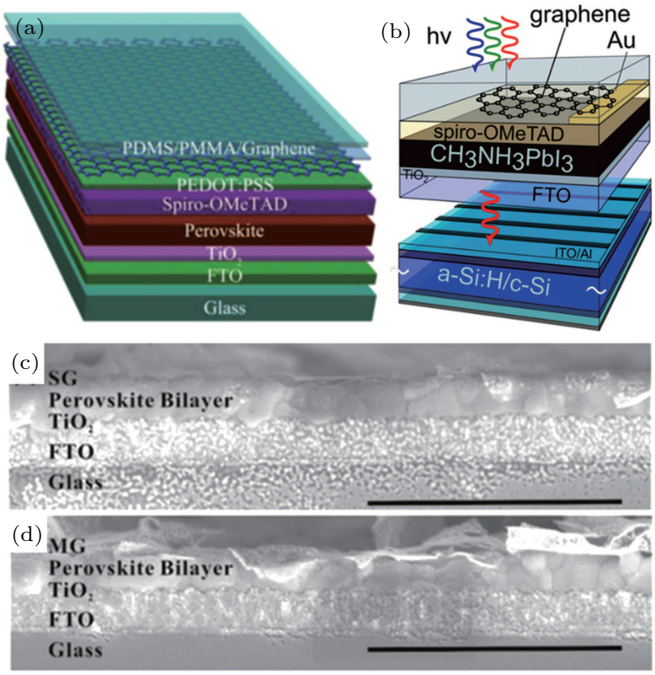


Fig. 16. (color online) (a) Schematic diagram of a semitransparent perovskite solar cell. Reprinted from Ref. [111]. (b) Simplified sketch of a four-terminal tandem solar cell consisting of a graphene-based perovskite top solar cell and an amorphous/crystalline silicon bottom solar cell. Reprinted from Ref. [112]. Solar cell performance using SG and MG for hole extraction. Cross-section view of (c) SG and (d) MG based PVSC (scale bar: 1 μm). Reprinted from Ref [76].

Hu *et al.* reported a three-dimensional honeycomb-like structured graphene (3DHG) synthesized by the reaction of potassium with CO_2.[75] HTM-free PVSCs introduced this 3DHG as counter electrode achieved a PCE of 10.06%. To complete the HTM-free device, 3DHG was coated atop a $CH_3NH_3PbI_3$ layer by doctor blading. Aiming to improve the interface, the 3DHG was dispersed into the solution of the perovskite precursors, and the perovskite layer was *in situ* synthesized. Consequently, a transition layer, in which part of $CH_3NH_3PbI_3$ perovskite molecules was highly scattered by ultrasonic on 3DHG, was formed between the perovskite layer and the 3DHG counter electrode. Common hysteresis effect was not observed for this device, as shown in Table 5.

Table 5. Photovoltaic performance of PVSCs with 3DHG-48 as the CE. Reprinted from Ref. [75].

CEs	J_{SC}/mA·cm^{-2}	V_{OC}/V	FF	Efficiency/%
Reverse	18.11	0.89	0.63	10.06
Forward	18.86	0.86	0.61	9.84

PVSCs with transparent contacts also used to compensate for thermalization losses of silicon solar cells in tandem devices which surpass the Schockley–Queisser limit for single-junction solar cells. PVSCs with large-area chemical vapor deposition (CVD)-graphene were fabricated by Nickel *et al.* for tandem solar cells, as shown in Fig. 16(b).[112] The performance of the device with a configuration of glass/FTO/TiO_2/$CH_3NH_3PbI_3$/spiro-OMeTAD/graphene is comparable to that of PVSCs with regular Au contact. The PCE of the tandem device was 13.2%, thus increased by 30% as compared to the respective perovskite single-junction cell.

3. Carbon materials for large area solar module

Most of the devices above have a small active area of around 0.1 cm^2. However, as a market-proof photovoltaic technology solution, one needs to demonstrate solar modules with larger area. To make solar panels with conventional structure employing layer-by-layer process, it is challenging to obtain large-area, flat, uniform, and fully covered perovskite films. To solve the problem, we deposited perovskites by slot-die coating technique assisted with our previously reported gas-pumping method (Figs. 17(a) and 17(b)).[113,114] In the end, carbon paste was screen-printed on top of the perovskite film as counter electrode. The as-prepared 5 cm×5 cm module showed a PCE of 10.6% and good stability over 140 days of outdoor testing.[115]

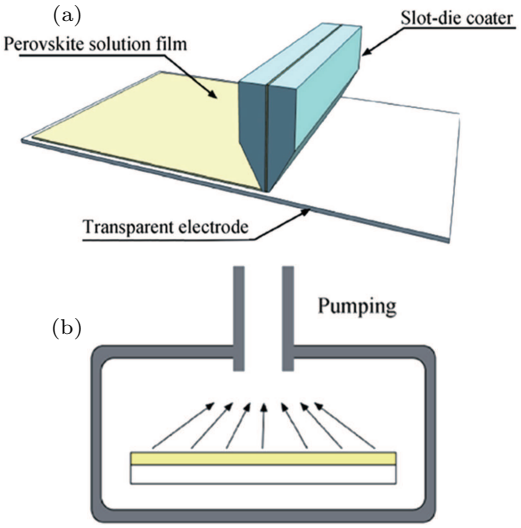


Fig. 17. (color online) (a) Schematic diagram of slot-die coating and (b) pumping of perovskite liquid film. Reprinted from Ref. [115].

In 2016, Mhaisalkar *et al.* reported monolithic perovskite modules with active areas of 70 cm^2. The module was fabricated by screen printing along with infiltration of the perovskite $(5\text{-AVA})_x(MA)_{1-x}PbI_3$ solution, showing a PCE of 10.74% and good ambient stability of over 2000 h with less than 5% reduction in efficiency. They pointed out that the quality of mesoscopic carbon has a significant impact on the module performance, where high Brunauer–Emmett–Teller (BET) surface area and low electrical resistance are propitious for achieving an efficient module.[116]

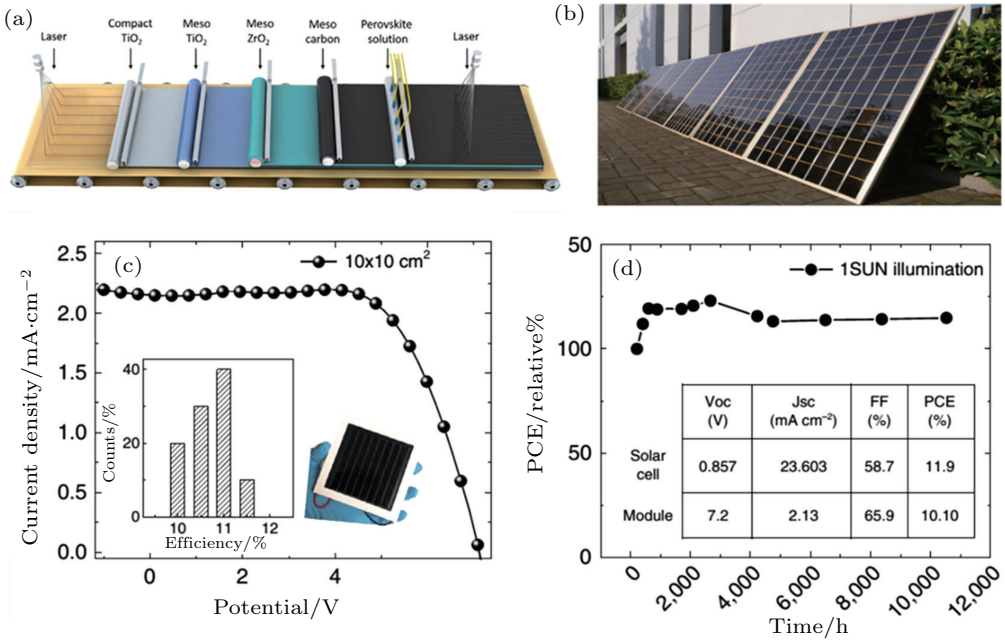


Fig. 18. (color online) (a) Schematic illustration of the proposed production line of perovskite solar modules. (b) Image of 7 m^2 printable perovskite solar panels. Reprinted from Ref. [117]. 2D/3D carbon based solar cell characteristics and stability. (c) *J–V* curve using the 2D/3D perovskite with 3%AVAI in an HTM-free 10 cm×10 cm module (device statistics and picture in the inset). (d) Typical module stability test under 1 sun AM 1.5 G conditions at stabilized temperature of 55 °C and short circuit conditions. Stability measurements were done according to the standard aging conditions. Reprinted from Ref. [118].

Later, employing the same structure, Han *et al.* optimized the thickness of the mesoporous TiO_2 and ZrO_2 layer and fabricated a large-area module (active area of 49 cm^2 out of total 100 cm^2) with a PCE of 10.4%. The module was stable under light soaking test with AM1.5 illumination for 1000 h and tested for a month under outdoor conditions. The shelf life under ambient conditions in the dark was over 1 year. Moreover, to assess the reproducibility of their screen-printing technique in manufacturing high-performance perovskite solar modules, a 7 m^2 fully printed perovskite solar panel was also demonstrated (Figs. 18(a) and 18(b)).[117]

Recently, Nazeeruddin *et al.* successfully fabricated 10 cm×10 cm (active area of 47.6 cm^2) monolithic structure modules with a fully printable industrial-scale process, showing the efficiency of 11.2%. More importantly, the sealed module kept stable for one-year (> 10000 h) under 1 sun AM 1.5 G illumination conditions at a stabilized temperature of 55 °C (Figs. 18(c) and 18(d)). They ascribed their ultra-stable solar cells to using mixed-cation perovskite of $(5AVA)_2PbI_4$ and $CH_3NH_3PbI_3$, which could form 2D/3D interfaces in the devices. Moreover, the 2D perovskite $(5AVA)_2PbI_4$ acts as a protective window against moisture, preserving the 3D perovskite.[118] These reports on large-area modules demonstrated the potential of carbon-based PVSCs to make up-scale production and paved the way to commercialization of perovskite solar cells.

4. Summary and outlook

CE is a crucial component of PVSCs, in this review, we introduce some critical works in the field of PVSCs that focus on designing or modifying cost-effective carbon-based CEs. After summing up this work, we find that there are mainly three key factors, included the electrical conductivity, the closeness of the perovskite (or HTM)/CE interface and matching work function that determine the performance of CEs and therefore the overall performance of the devices. Carbon materials attracted quite a few researchers because of their earth-abundant, low-cost, and decent conductive properties. Carbon materials can be deposited on the top of the as-prepared substrate by different methods such as screen printing, doctor-blading, inkjet-printing, rolling transfer, hot pressing, spin coating, press transferring, and drop-casting. Although this kind of CEs often have a poor contact with perovskite or HTM, different approaches such as doping, morphology tuning, and device engineering have been used to alleviate this problem and improve the performance of carbon-PVSCs. Among the carbon materials, CNTs and graphene

stand out to be potential candidate CEs for semi-transparent or transparent PVSCs, which can be employed in building-integrated photovoltaics and tandem solar cells. Moreover, device lifetime up to 3000 hours has been reported based on carbon cell. A comparison of the device performance between different types of carbon-based CEs is visualized in Fig. 19(a). Firstly, it is clear that more efforts were put on the use of standard carbon paste due to the easy availability and low cost. The highest PCE was also achieved from the device with carbon paste based CEs. Relatively lower PCEs and fewer reports on the CNT and graphene based devices could be due to the emphasis on the transparency of these types of solar cells. In Fig. 19(b), we attempted to plot the FF values from two main kinds of devices based carbon pastes: monolithic and conventional. Generally, the former structure has higher FF than the latter, possibility due to better contact and lower resistance of the monolithic structures. The progress of large-area modules based on carbon CEs were also presented, and the potential of scaling up PVSCs with carbon CEs was confirmed.

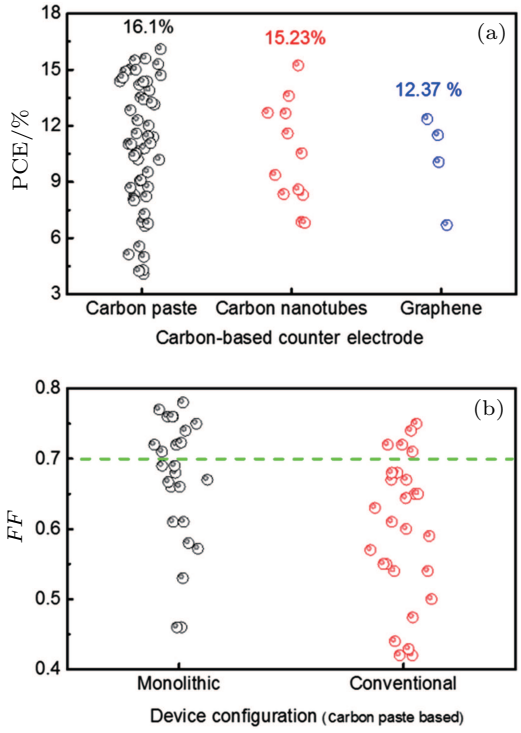


Fig. 19. (color online) Comparison of the performance of the devices with (a) different types of carbon-based counter electrodes and (b) different types of device structures (data were analyzed based on Table 1).

It is evident that there is still a huge gap in PCEs between the carbon-based devices and noble metal-based devices. There is also an ample space for improving the device performance if we can further increase the conductivity of the carbon electrode and improve the contact between the electrode and charge-selective contacts. On the other hand, traditional PVSCs employing noble metals as CEs usually need organic HTMs such as spiro-OMeTAD, PTAA, and PEDOT:PSS, which deteriorate device stability under high humidity or high-temperature conditions. However, the carbon-based devices such as monolithic devices or devices using CNTs as HTM can avoid the use of these fragile organic compounds, and therefore the moist and thermal stability can be enhanced. More importantly, a relatively large-area module with a lifetime up to 10000 hours has been reported based on HTM-free carbon cells. Thus, given the low cost and long-term stability of the carbon materials, they can be an essential solution for the commercialization of perovskite solar cells.

References

[1] Green M A 2001 *Prog. Photovoltaics Res. Appl.* **9** 123
[2] Shen Y, Chen J, Yang J, Chen B, Chen J, Li F, Dai X, Liu H, Xu Y and Mai Y 2016 *Chin. Phys. B* **25** 118801
[3] Li T, Zhou C L and Wang W J 2016 *Chin. Phys. Lett.* **33** 38801
[4] Li T and Wang W J 2015 *Chin. Phys. Lett.* **32** 28801
[5] Xu W W 2012 *Acta Phys. Sin.* **61** 88801 (in Chinese)
[6] Kojima A, Teshima K, Shirai Y and Miyasaka T 2009 *J. Am. Chem. Soc.* **131** 6050
[7] Liu P, LiuG, Wu R, Zhang C, Wan F, LiS, Yang J, GaoY and Zhou B Y 2017 *Chin. Phys. B* **26** 58401
[8] Du H J, Wang W C and Gu Y F 2017 *Chin. Phys. B* **26** 28803
[9] Xia C, Song W D, Zhang C Z, Yuan S Y, Hu W X, Qin P, Wang R P, Zhao L L, Wang X F, He M and Li S T 2017 *Chin. Phys. B* **26** 18401
[10] Correa-Baena J P, Abate A, Saliba M, Tress W, Jesper Jacobsson T, Grätzel M and Hagfeldt A 2017 *Energy Environ. Sci.* **10** 710
[11] Gao P, Grätzel M and Nazeeruddin M K 2014 *Energy Environ. Sci.* **7** 2448
[12] Gao P, Konrad D, Aghazada S and Nazeeruddin M K 2015 *Chim. Int. J. Chem.* **69** 253
[13] Saparov B and Mitzi D B 2016 *Chem. Rev.* **116** 4558
[14] Yang W S, Park B W, Jung E H, Jeon N J, Kim Y C, Lee D U, Shin S S, Seo J, Kim E K, Noh J H and Seok S Il 2017 *Science* **356** 1376
[15] Wilks R G and Bär M 2017 *Nat. Energy* **2** 16204
[16] Domanski K, Correa-Baena J P, Mine N, Nazeeruddin M K, Abate A, Saliba M, Tress W, Hagfeldt A and Grätzel M 2016 *ACS Nano* **10** 6306
[17] Leijtens T, Eperon G E, Pathak S, Abate A, Lee M M and Snaith H J 2013 *Nat. Commun.* **4** 2885
[18] Ku Z, Rong Y, Xu M, Liu T and Han H 2013 *Sci. Rep.* **3** 3132
[19] Wei Z, Chen H, Yan K and Yang S 2014 *Angew. Chemie Int. Ed.* **53** 13239
[20] Yang Y, Xiao J, Wei H, Zhu L, Li D, Luo Y, Wu H and Meng Q 2014 *RSC Adv.* **4** 52825
[21] Zhang F, Yang X, Wang H, Cheng M, Zhao J H J and Sun L 2014 *ACS Appl. Mater. Interfaces* **6** 16140
[22] Zhou H, Shi Y, Dong Q, Zhang H, Xing Y, Wang K, Du Y and Ma T 2014 *J. Phys. Chem. Lett.* **5** 3241
[23] Mei A, Li X, Liu L, Ku Z, Liu T, Rong Y, Xu M, Hu M, Chen J, Yang Y, Gratzel M and Han H 2014 *Science* **345** 295
[24] Rong Y, Ku Z, Mei A, Liu T, Xu M, Ko S, Li X and Han H 2014 *J. Phys. Chem. Lett.* **5** 2160
[25] Cao K, Zuo Z, Cui J, Shen Y, Moehl T, Zakeeruddin S M, Grätzel M and Wang M 2015 *Nano Energy* **17** 171
[26] Liu T, Liu L, Hu M, Yang Y, Zhang L, Mei A and Han H 2015 *J. Power Sources* **293** 533
[27] Wei H, Xiao J, Yang Y, Lv S, Shi J, Xu X, Dong J, Luo Y, Li D and Meng Q 2015 *Carbon* **93** 861
[28] Zhou H, Shi Y, Wang K, Dong Q, Bai X, Xing Y, Du Y and Ma T 2015 *J. Phys. Chem. C* **119** 4600
[29] Liu Z, Zhang M, Xu X, Bu L, Zhang W, Li W, Zhao Z, Wang M, Cheng Y B and He H 2015 *Dalt. Trans.* **44** 3967
[30] Zhang F, Yang X, Cheng M, Li J, Wang W, Wang H and Sun L 2015 *J. Mater. Chem. A* **3** 24272
[31] Xu X, Liu Z, Zuo Z, Zhang M, Zhao Z, Shen Y, Zhou H, Chen Q, Yang Y and Wang M 2015 *Nano Lett.* **15** 2402
[32] Li H, Cao K, Cui J, Liu S, Qiao X, Shen Y and Wang M 2016 *Nanoscale* **8** 6379

[33] Liu Z, Sun B, Shi T, Tang Z and Liao G 2016 *J. Mater. Chem. A* **4** 10700

[34] Tsai C M, Wu H P, Chang S T, Huang C F, Wang C H, Narra S, Yang Y W, Wang C L, Hung C H and Diau E W G 2016 *ACS Energy Lett.* **1** 1086

[35] Wang B X, Liu T F, Zhou Y B, Chen X, Yuan X B, Yang Y Y, Liu W P, Wang J M, Han H W and Tang Y W 2016 *Phys. Chem. Chem. Phys.* **18** 27078

[36] Zhang N, Guo Y, Yin X, He M and Zou X 2016 *Mater. Lett.* **182** 248

[37] Chan C Y, Wang Y, Wu G W and Diau E W G 2016 *J. Mater. Chem. A* **4** 3872

[38] Liu Z, Shi T, Tang Z, Sun B and Liao G 2016 *Nanoscale* **8** 7017

[39] Yue G, Chen D, Wang P, Zhang J, Hu Z and Zhu Y 2016 *Electrochim. Acta* **218** 84

[40] Zhang C, Luo Y, Chen X, Chen Y, Sun Z and Huang S 2016 *Nano-Micro Lett.* **8** 347

[41] Chen H N, Wei Z H, He H X, Zheng X L, Wong K S and Yang S H 2016 *Adv. Energy Mater.* **6** 1502087

[42] Gholipour S, Correa-Baena J P, Domanski K, Matsui T, Steier L, Giordano F, Tajabadi F, Tress W, Saliba M, Abate A, Morteza Ali A, Taghavinia N, Grätzel M and Hagfeldt A 2016 *Adv. Energy Mater.* **6** 1601116

[43] Chang X, Li W, Chen H, Zhu L, Liu H, Geng H, Xiang S, Liu J, Zheng X, Yang Y and Yang S 2016 *ACS Appl. Mater. Interfaces* **8** 30184

[44] Tsai C, Wu G, Narra S, Chang H, Mohanta N, Wu H P, Wang C L and Diau E W G 2017 *J. Mater. Chem. A* **5** 739

[45] Hashmi S G, Martineau D, Li X, Ozkan M, Tiihonen A, Dar M I, Sarikka T, Zakeeruddin S M, Paltakari J, Lund P D and Grätzel M 2017 *Adv. Mater. Technol.* **2** 1600183

[46] Xu L, Wan F, Rong Y, Chen H, He S, Xu X, Liu G, Han H, Yuan Y, Yang J, Gao Y, Yang B and Zhou C 2017 *Org. Electron.* **45** 131

[47] Chen M, Zha R H, Yuan Z Y, Jing Q S, Huang Z Y, Yang X K, Yang S M, Zhao X H, Xu D L and Zou G D 2017 *Chem. Eng. J.* **313** 791

[48] Liu Z, Zhang M, Xu X, Bu L, Zhang W, Li W, Zhao Z, Wang M, Cheng Y B and He H 2015 *Dalt. Trans.* **44** 3967

[49] Xiao Y, Cheng N, Kondamareddy K K, Wang C, Liu P, Guo S and Zhao X Z 2017 *J. Power Sources* **342** 489

[50] Zhang F, Yang X, Cheng M, Wang W and Sun L 2016 *Nano Energy* **20** 108

[51] Yang Y, Ri K, Mei A, Liu L, Hu M, Liu T, Li X and Han H 2015 *J. Mater. Chem. A* **3** 9103

[52] Chen J, Xiong Y, Rong Y, Mei A, Sheng Y, Jiang P, Hu Y, Li X and Han H 2016 *Nano Energy* **27** 130

[53] Rong Y, Hou X, Hu Y, Mei A, Liu L, Wang P and Han H 2017 *Nat. Commun.* **8** 14555

[54] Chen H, Zheng X, Li Q, Yang Y, Xiao S, Hu C, Bai Y, Zhang T, Wong K S and Yang S 2016 *J. Mater. Chem. A* **4** 12897

[55] Chang X, Li W, Zhu L, Liu H, Geng H, Xiang S, Liu J and Chen H 2016 *ACS Appl. Mater. Interfaces* **8** 33649

[56] Li J, Yao J X, Liao X Y, Yu R L, Xia H R, Sun W T, Peng L M, Wu H, Li D, Luo Y, Meng Q, Han H and Snaith H J 2017 *RSC Adv.* **7** 20732

[57] Chen H, Wei Z, Zheng X and Yang S 2015 *Nano Energy* **15** 216

[58] He X, Bai Y, Chen H, Zheng X and Yang S 2016 *MRS Adv.* **1** 3175

[59] Hou X, Hu Y, Liu H, Mei A, Li X, Duan M, Zhang G, Rong Y and Han H 2017 *J. Mater. Chem. A* **5** 73

[60] Cao K, Cui J, Zhang H, Li H, Song J K, Shen Y, Cheng Y B and Wang M K 2015 *J. Mater. Chem. A* **3** 9116

[61] Chen J, Rong Y, Mei A, Xiong Y, Liu T, Sheng Y, Jiang P, Hong L, Guan Y, Zhu X, Hou X, Duan M, Zhao J, Li X and Han H 2016 *Adv. Energy Mater.* **6** 1502009

[62] Wei Z, Yan K, Chen H, Yi Y, Zhang T, Long X, Li J, Zhang L, Wang J and Yang S 2014 *Energy Environ. Sci.* **7** 3326

[63] Li J, Niu G, Li W, Cao K, Wang M and Wang L 2016 **131** 6050

[64] Xu X, Zhang H, Cao K, Cui J, Lu J, Zeng X, Shen Y and Wang M 2014 *ChemSusChem* **7** 3088

[65] Nouri E, Mohammadi M R and Lianos P 2017 *Chem. Commun.* **53** 1630

[66] Li Z, Kulkarni S A, Boix P P, Shi E, Cao A, Fu K, Batabyal S K, Zhang J, Xiong Q, Wong L H, Mathews N and Mhaisalkar S G 2014 *ACS Nano* **8** 6797

[67] Wang X, Li Z, Xu W, Kulkarni S A, Batabyal S K, Zhang S, Cao A and Wong L H 2015 *Nano Energy* **11** 728

[68] Aitola K, Sveinbjornsson K, Correa Baena J P, Kaskela A, Abate A, Tian Y, Johansson E M J, Grätzel M, Kauppinen E, Hagfeldt A and Boschloo G 2015 *Energy Environ. Sci.* **9** 461

[69] Luo Q, Ma H, Zhang Y, Yin X, Yao Z, Wang N, Li J, Fan S, Jiang K and Lin H 2016 *J. Mater. Chem. A* **4** 5569

[70] Cheng N, Liu P, Qi F, Xiao Y, Yu W, Yu Z, Liu W, Guo S S and Zhao X Z 2016 *J. Power Sources* **332** 24

[71] Zheng X, Chen H, Li Q, Yang Y, Wei Z, Bai Y, Qiu Y, Zhou D, Wong K S and Yang S 2017 *Nano Lett.* **17** 2496

[72] Wei Z, Chen H, Yan K, Zheng X and Yang S 2015 *J. Mater. Chem. A* **3** 24226

[73] Liu S, Cao K, Li H, Song J, Han J, Shen Y and Wang M 2017 *Sol. Energy* **144** 158

[74] You P, Liu Z, Tai Q, Liu S and Yan F 2015 *Adv. Mater.* **27** 3632

[75] Wei W, Hu B, Jin F, Jing Z, Li Y, García Blanco A A, Stacchiola D J and Hu Y H 2017 *J. Mater. Chem. A* **5** 7749

[76] Yan K, Wei Z, Li J, Chen H, Yi Y, Zheng X, Long X, Wang Z, Wang J, Xu J and Yang S 2015 *Small* **11** 2269

[77] McCreery R L 2008 *Chem. Rev.* **108** 2646

[78] Hu R, Chu L, Zhang J and Huang W 2017 *J. Power Sources* **361** 259

[79] Kay A and Grätzel M 1996 *Sol. Energy Mater. Sol. Cells* **44** 99

[80] Zhang L, Liu T, Liu L, Hu M, Yang Y, Mei A and Han H 2015 *J. Mater. Chem. A* **3** 9165

[81] Sutton R J, Eperon G E, Miranda L, Parrott E S, Kamino B A, Patel J B, Hörantner M T, Johnston M B, Haghighirad A A, Moore D T and Snaith H J 2016 *Adv. Energy Mater.* **6** 1502458

[82] Beal R E, Slotcavage D J, Leijtens T, Bowring A R, Belisle R A, Nguyen W H, Burkhard G F, Hoke E T and McGehee M D 2016 *J. Phys. Chem. Lett.* **7** 746

[83] Kulbak M, Cahen D and Hodes G 2015 *J. Phys. Chem. Lett.* **6** 2452

[84] Li W, Li J, Li J, Fan J and Wang L 2016 *J. Mater. Chem. A* **4** 17104

[85] Zhou H, Shi Y, Dong Q, Zhang H, Xing Y, Wang K, Du Y and Ma T 2014 *J. Phys. Chem. Lett.* **5** 3241

[86] Iijima S 1991 *Nature* **354** 56

[87] Habisreutinger S N, Nicholas R J and Snaith H J 2017 *Adv. Energy Mater.* **7** 1601839

[88] Wang F, Kozawa D, Miyauchi Y, Hiraoka K, Mouri S, Ohno Y and Matsuda K 2015 *Nat. Commun.* **6** 6305

[89] Ryu J, Lee K, Yun J, Yu H, Lee J and Jang J 2017 *Small* **13** 1701225

[90] Aitola K, Domanski K, Correa-Baena J P, Sveinbjörnsson K, Saliba M, Abate A, Grätzel M, Kauppinen E, Johansson E M J, Tress W, Hagfeldt A and Boschloo G 2017 *Adv. Mater.* **29** 1606398

[91] Novoselov1 K S, Geim1 A K, Morozov S V, Jiang D, Zhang Y, Dubonos S V, Grigorieva1 I V, Firsov A A 2004 *Science* **306** 666

[92] Yin Z, Zhu J, He Q, Cao X, Tan C, Chen H, Yan Q and Zhang H 2014 *Adv. Energy Mater.* **4** 1300574

[93] Bouclé J and Herlin-Boime N 2015 *Synth. Met.* **222** 3

[94] Liu Z, Lau S P and Yan F 2015 *Chem. Soc. Rev.* **44** 5638

[95] Acik M and Darling S B 2016 *J. Mater. Chem. A* **4** 6185

[96] Wang J T W, Ball J M, Barea E M, Abate A, Alexander-Webber J A, Huang J, Saliba M, Mora-Sero I, Bisquert J, Snaith H J and Nicholas R J 2014 *Nano Lett.* **14** 724

[97] Liu Z, You P, Xie C, Tang G and Yan F 2016 *Nano Energy* **28** 151

[98] Sung H, Ahn N, Jang M S, Lee J K, Yoon H, Park N G and Choi M 2016 *Adv. Energy Mater.* **6** 1501873

[99] Yoon J, Sung H, Lee G, Cho W, Ahn N, Jung H S and Choi M 2017 *Energy Environ. Sci.* **10** 337

[100] Wu Z, Bai S, Xiang J, Yuan Z, Yang Y, Cui W, Gao X, Liu Z, Jin Y and Sun B 2014 *Nanoscale* **6** 10505

[101] Yeo J S, Kang R, Lee S, Jeon Y J, Myoung N, Lee C L, Kim D Y, Yun J M, Seo Y H, Kim S S and Na S I 2015 *Nano Energy* **12** 96

[102] Cao J, Liu Y, Jing X, Yin J, Li J, Xu B, Tan Y and Zheng N 2015 *J. Am. Chem. Soc.* **137** 10914

[103] Huang X, Guo H, Yang J, Wang K, Niu X and Liu X 2016 *Org. Electron. Phys. Mater. Appl.* **39** 288

[104] Giuri A, Masi S, Colella S, Listorti A, Rizzo A, Gigli G, Liscio A, Treossi E, Palermo V, Rella S, Malitesta C and Esposito Corcione C 2016 *IEEE Trans. Nanotechnol.* **15** 725

[105] Kim J, Teridi M A M and Yusoff A R 2016 *Sci. Rep.* **6** 27773

[106] Li D, Cui J, Li H, Huang D, Wang M and Shen Y 2016 *Sol. Energy* **131** 176

[107] Eperon G E, Burlakov V M, Goriely A and Snaith H J 2014 *ACS Nano* **8** 591

[108] Roldán-Carmona C, Malinkiewicz O, Betancur R, Longo G, Momblona C, Jaramillo F, Camacho L and Bolink H J 2014 *Energy Environ. Sci.* **7** 2968

[109] Eperon G E, Bryant D, Troughton J, Stranks S D, Johnston M B, Watson T, Worsley D A and Snaith H J 2015 *J. Phys. Chem. Lett.* **6** 129

[110] Bryant D, Greenwood P, Troughton J, Wijdekop M, Carnie M, Davies M, Wojciechowski K, Snaith H J, Watson T and Worsley D 2014 *Adv. Mater.* **26** 7499

[111] You P, Liu Z, Tai Q, Liu S and Yan F 2015 *Adv. Mater.* **27** 3632

[112] Lang F, Gluba M A, Albrecht S, Rappich J, Korte L, Rech B and Nickel N H 2015 *J. Phys. Chem. Lett.* **6** 2745

[113] Gao L L, Liang L, Song X X, Ding B, Yang G J, Fan B, Li C C and Li C C 2016 *J. Mater. Chem. A* **4** 3704

[114] Ding B, Gao L, Liang L, Chu Q, Song X, Li Y, Yang G, Fan B, Wang M, Li C and Li C 2016 *ACS Appl. Mater. Interfaces* **8** 20067

[115] Cai L, Liang L, Wu J, Ding B, Gao L and Fan B 2017 *J. Semicond.* **38** 14006

[116] Priyadarshi A, Haur L J, Murray P, Fu D, Kulkarni S, Xing G, Sum T C, Mathews N and Mhaisalkar S G 2016 *Energy Environ. Sci.* **9** 3687

[117] Hu Y, Si S, Mei A, Rong Y, Liu H, Li X and Han H 2017 *Sol. RRL* **1** 1600019

[118] Grancini G, Roldán-Carmona C, Zimmermann I, Mosconi E, Lee X, Martineau D, Narbey S, Oswald F, De Angelis F, Graetzel M and Nazeeruddin M K 2017 *Nat. Commun.* **8** 15684